JOURNAL OF GEOPHYSICAL RESEARCH, VOL. 95, NO. B5, PAGES 6799-6827, MAY 10, 1990

Modeling of Residual Spheres for Subduction Zone Earthquakes 1. Apparent Slab Penetration Signatures in the NW Pacific Caused by Deep Diffuse Mantle Anomalies

HUA-WEI ZHOU [1], DON L. ANDERSON, AND ROBERT W. CLAYTON

Seismological Laboratory, California Institute of Technology, Pasadena

We have computed focal residual spheres for 145 subduction zone earthquakes along the northwest edge of the Pacific using regional and global mantle velocity models from tomographic inversions. The mantle models explain much of the observed residual sphere data and, to a certain extent, suggest the location of mantle velocity heterogeneities which are responsible for various residual sphere patterns. For most deep events considered, the fast slablike residual sphere anomalies are caused by diffuse heterogeneities, mainly of deep lower mantle and receiver mantle origin rather than by an extension of the slab. The region immediately below the deepest earthquakes, depths of 650-1500 km, has an effect usually smaller than or comparable to the effect of other regions of the mantle. Without a proper account of the teleseismic effect, attributing the long-wavelength anomalies of the residual sphere to near-source slab effects alone, or even primarily, is not valid. The fast bands in many observed residual spheres agree with seismicity trends. Once the deep mantle and receiver mantle effects are removed, these may give the approximate orientation, but not the depth extent, of near-source fast velocities. For most deep earthquakes under Japan the predominant fast band is subhorizontal rather than near vertical. This type feature would be overlooked in conventional residual sphere studies using only steeply diving rays and cosine weighting of the data.

1. INTRODUCTION

The residual sphere [*Davies and McKenzie*, 1969] is the focal sphere projection of travel time residuals of an earthquake and represents graphically the accumulated mantle heterogeneity traversed by all rays. Travel times of seismic waves from a deep focus earthquake are plotted on an imaginary sphere surrounding the earthquake. Each ray penetrates this sphere at a specific point, which depends on the azimuth and distance between the event and the station In practice, the difference between the travel time of the ray and the travel time in a reference Earth model is plotted on a lower hemisphere projection. Thus the steepest rays and those travelling to the most distant stations are plotted near the center of the hemisphere, and rays leaving the source horizontally are plotted on the boundary of the hemisphere.

The residual spheres of deep subduction zone earthquakes are particularly interesting since they have been used to study the depth of the subducting lithospheric slab, a problem basic to our understanding of mantle convection, evolution of subduction zones, and general plate tectonics. Previous studies of residual spheres of a few deep subduction zone earthquakes [*Jordan*, 1977; *Creager and Jordan*, 1984, 1986] have been used to argue for penetration of the lithospheric slab deep into the lower mantle

Deep focus earthquakes are generally assumed to be embedded in cold subducted slabs with high seismic velocities. High-velocity slabs act as antiwaveguides, causing seismic energy to defocus and to leave the slab. By contrast, seismic wave energy can be trapped in low-velocity channels, or waveguides, and can travel for large distances in the channel. Nevertheless, it has been proposed that 1- to 2-s travel time anomalies from deep focus earthquakes are due to long distance propagation in high-velocity slabs [*Creager and Jordan*, 1984]. A slab related velocity anomaly of 5% thus corresponds to slab propagation paths of 200-400 km. Alternatively, the observed travel time anomaly may be accumulated in the deeper mantle, since teleseismic rays spend most of their time there, or near the receiver, since the upper mantle is extremely inhomogeneous.

The travel times of seismic waves to teleseismic stations are of the order of 1000 s. Long-wavelength velocity anomalies of only 0.5% can therefore lead to travel time residuals of 5 s. Observed travel time residuals of deep focus earthquakes, after smoothing, are of the order of 1-2 s Seismic waves from deep focus earthquakes recorded at distant stations spend of the order of 2-4% of their travel time in the region where deep slab penetration has been hypothesized, i.e., the upper mantle and the top part of the lower mantle under the source. Since large-scale coherent

[1] Now at Department of Geosciences, University of Houston, Houston, Texas.

Paper number 89JB03215.
0148-0227/90/89JB-03215$05.00

velocity anomalies of the order of 0.5% or larger in the lower mantle are available [e.g., *Hager et al.*, 1985; *Dziewonski and Woodhouse*, 1987] and that station correction terms usually do not fully account for receiver upper mantle, it would seem to be difficult to extract evidence for deep slab penetration from teleseismic data. In particular, seismic rays from deep focus earthquakes are well spread out at lower mantle depths, especially if they are defocused near the origin by fast slab "antiwaveguides".

A major task of this paper is to investigate the limitation of the residual sphere method in constraining the morphology of subducted slabs. We are primarily interested in the effect of the deep mantle on residual spheres By "deep mantle" we mean the mantle between a depth of 1500 km at the source side of the seismic ray, to the surface at the receiver site. Thus we mask out the part of the mantle where previous investigations have assumed a cold, fast slab to be. If the travel time residuals for wave propagation in the deep mantle project onto the residual sphere as a fast band or if they are of high amplitude, then it would be difficult to argue for a near-source deep slab structure in observed data.

Upper (Moho to 650 km) and middle mantle (650-1500 km) models are now available for many subduction zones so we can also calculate the accumulated travel time anomaly, or residual, for these parts of the mantle. We can then compare observed residual spheres with the component, as well as total, computed residual spheres. In particular, we attempt to relate the location of mantle heterogeneities responsible for features in the observed residual spheres by analyzing predicted residual spheres based on three-dimensional mantle velocity models obtained from inversions of International Seismological Centre (ISC) travel time delays

Creager and Jordan [1986] corrected lower mantle heterogeneity from residual data using *Dziewonski*'s [1984] degree 6 aspherical model L02 56 The present study uses a *P* wave mantle model by *Clayton and Comer* [1983], which has been documented by *Hager and Clayton* [1989] Our choice is based mainly on two points. First, *Dziewonski* [1984] has made it clear, by comparing the observed travel time anomalies with the predicted from L02 56, that L02 56 usually underpredicts the amplitude of the anomalies but predicts the sign well He reasonably attributed the low amplitude of his model to the fact that only a low-pass-filtered image of the Earth's interior has been recovered The Clayton-Comer model usually has an amplitude 1-2 times that of model L02.56 at most lower mantle depths Second, L02 56 is a lower mantle only model, while the Clayton-Comer model also includes most of the near-receiver upper mantle. Given the fact that near-receiver upper mantle can be as heterogeneous as the source mantle and that station corrections, in most cases, represent only shallow heterogeneities, we feel that our choice more accurately accounts for the teleseismic contribution. *Dziewonski and Anderson* [1983] attempted to address near-receiver upper mantle more precisely by introducing azimuth-dependent correction terms. Creager and Jordan's work corrected only for the azimuth-independent term.

In addition, we used a regional model covering the upper mantle and upper half of the lower mantle around the northwest Pacific subduction zones [*Zhou and Clayton*, 1987, 1990]. These mantle models, although possibly unrealistic in some respects, may help to relate residual sphere anomalies to specific mantle heterogeneities. For instance, most lower mantle tomographic models exhibit a broad band of high velocities surrounding the Pacific, thus giving a fast band on residual spheres which has approximately the orientation of the seismic zone. This band is more than 5000 km broad but projects onto the residual sphere as a narrow band that could be confused with, or dominate, a similar band caused by near-source effects.

2. DATA

Our basic plan is to calculate the contribution to the residual sphere from upper, middle and deep mantle models. Rather than just computing residual spheres at arbitrary locations and arbitrary depths we do the calculation at the hypocenters of the 145 best recorded NW Pacific earthquakes (Figure 1) in ISC catalogs between 1965 and 1982, so that we are able to compare the model prediction with observed residual spheres. These events include all 18 NW Pacific events analyzed by *Creager and Jordan* [1984, 1986]. As listed in Table 1, the events are composed of all earthquakes that have more than 240 *P* wave picks, plus the deepest Mariana event, event 3, focal depth 624 km by ISC. These events occurred in the major subduction zones of the northwest Pacific from 17°N to 54°N, with focal depth greater than 120 km. The selection criteria for them are that (1) source-receiver distance is short enough (less than about 98°) to avoid core interactions; and (2) after corrections, including source relocation, the observed travel times differ by less than 6 s from the Jeffreys-Bullen (JB) model times. The station residual averages obtained by Clayton and Comer [1983] are removed to correct for near receiver shallow structure. Furthermore, the data are corrected for Earth's ellipticity following *Dziewonski and Gilbert* [1976].

The predictions regarding the contributions to the theoretical residual spheres from different regions of the mantle velocity models depend on the reliability of the models utilized The predicted residual spheres are very similar for close-by events A source mislocation, on the other hand, changes the pattern and amplitude of the observed, or data, residual spheres. In terms of spherical harmonics, a mislocation or an error in origin time may be contained in the l=1 and 2, and l=0 terms, respectively (in a homogeneous Earth). The relocation process puts the average residual back into the origin time; hence there is little degree one term in the data It would be easy to isolate other terms by expanding the data with spherical harmonics and then omitting the offending terms However, an adequate spherical harmonic expansion requires a uniform and sufficient station coverage on the focal sphere, a situation which is unfortunately not available for most earthquakes. Poor coverage violates the orthogonality condition and hence causes aliasing. It is therefore impossible, for most events, to use an orthogonal expansion to separate the mislocation and origin time error terms

Consequently, the source relocation issue is treated separately with a conventional procedure. Later on in this paper, a spherical harmonic fitting is used, and can only be used, to provide a smoothed version of residual sphere

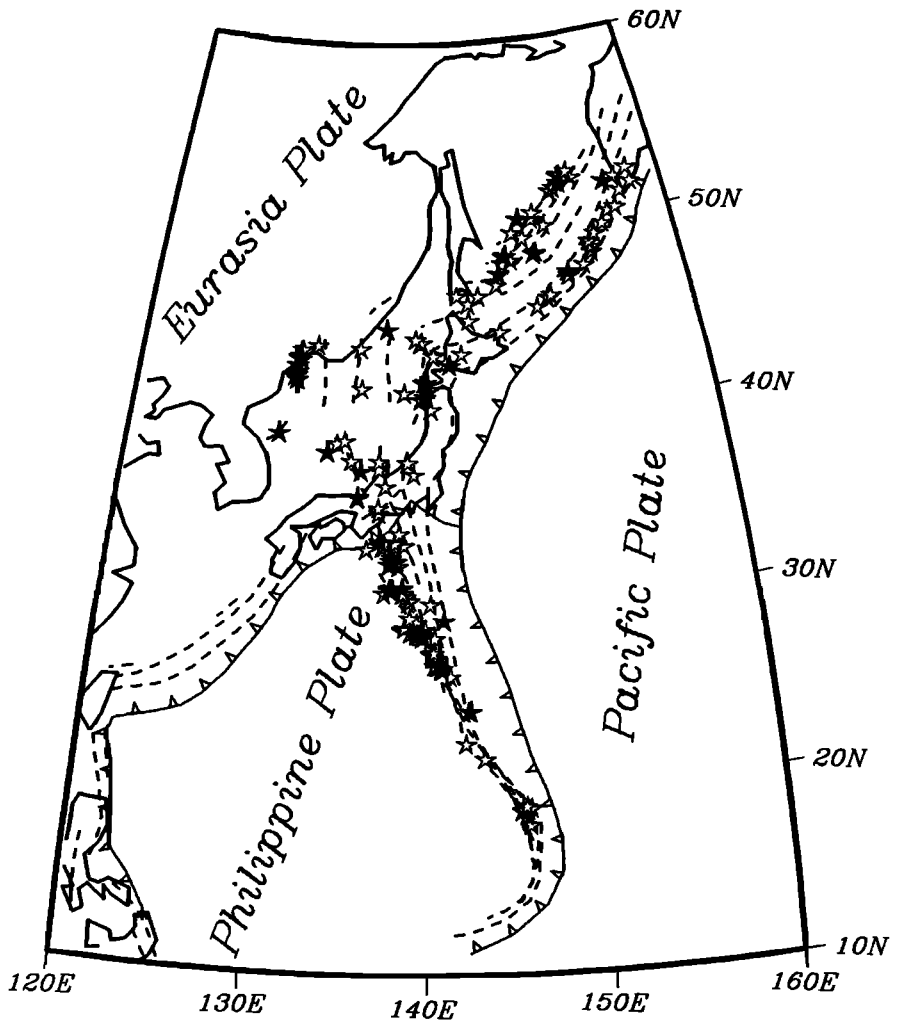

Fig. 1 Index map. The northwest Pacific region shown here is the location of the regional velocity model which covers the upper mantle and upper half of the lower mantle. The major NW Pacific subduction zone is shown in dashed contours at 100-km depth intervals. Solid and open stars are earthquakes utilized in this study. All events with more than 400 *P* wave arrivals, denoted by solid stars, are considered in a test shown in Figure 16.

anomalies for comparison purposes. The individual harmonic coefficients do not have a simple physical explanation, due to the above reason. Our major conclusions, including the relative amplitudes of the contributions from the middle and deep mantles, are based on the unsmoothed data. The effect of source location error on the model prediction, also contained in the degree one term, is much smaller than the effect on the observed data. This point will be addressed in detail in section 5.

The station coverage on residual spheres analyzed by Creager and Jordan is even poor than ours due to their exclusion of rays of greater than 60°, from the vertical, takeoff angle. Since an orthogonal expansion of a spherical data set cannot be constructed without adequate coverage on the focal sphere, their smoothing cannot be free of aliasing and may not remove the true degree one harmonic terms.

The source mislocation effect is of critical importance to recognizing a slab signature in observed residual spheres but is less essential to determining the location of mantle heterogeneities responsible for a given residual sphere pattern. To facilitate a more reliable comparison between the predicted and observed residual spheres, however, all the events in this study are relocated. Based on the observed travel times and the JB reference model, a standard source relocation scheme is applied using a linearization formula

$$dt_j = \delta t^o + (\frac{\partial t}{\partial \theta})_j \delta\theta + (\frac{\partial t}{\partial \phi})_j \delta\phi + (\frac{\partial t}{\partial h})_j \delta h + \epsilon$$

for the jth station, where dt_j is the observed travel time minus theoretical travel time, δt^o is a correction for the origin time, the next three terms are the corrections for the source location in terms of latitude θ, longitude ϕ, and depth h, and ϵ is error term. The gradients of t in each directions $(\partial t/\partial\theta)_j$, $(\partial t/\partial\phi)_j$ and $(\partial t/\partial h)_j$ are assumed to be linear, near the source, for each ray (depending on epicentral distance, focal depth, and the velocity structure).

TABLE 1. Source Parameters and Correlations Between Observed and Predicted Residual Spheres

Event	Date	Time, UT	Latitude °N	Longitude °E	Depth, km	m_b	$n^\dagger$	Correlation Coefficients‡			
								R_w	R_u	R_m	R_d
1	Jan. 4, 1982	0605:02.2(-0.4)	17.99(-0.00)	145.64(-0.02)	600(-8)	6.0	279	0.24	0.36	0.26	0.16
2	Oct. 17, 1979	0543:02.8(-0.3)	18.50(0.02)	145.43(0.04)	597(-3)	6.2	293	0.24	0.39	0.18	0.16
3*	July 3, 1972	0119:27.2(-0.1)	18.71(0.01)	145.15(0.06)	621(-3)	5.5	185	0.10	0.15	0.18	0.03
4*	Oct. 30, 1979	0137:06.7(0.2)	18.78(0.02)	145.21(0.06)	583(-2)	5.2	234	0.20	0.45	0.19	0.05
5	May 24, 1977	1023:26.0(-0.2)	18.80(0.02)	145.53(0.04)	230(-1)	5.5	270	0.43	0.39	0.38	0.34
6*	Jan. 25, 1974	2028:13.3(-0.4)	18.90(0.03)	145.69(0.06)	143(-6)	5.6	241	0.30	0.33	0.15	0.12
7*	May 13, 1979	0626:08.7(0.3)	19.00(-0.00)	145.44(0.03)	257(2)	6.2	268	0.37	0.32	0.21	0.32
8	Aug. 15, 1969	0841:55.3(0.5)	21.58(0.01)	143.15(0.05)	324(5)	5.9	222	0.27	0.04	0.37	0.28
9	Feb. 8, 1980	1307:14.4(0.0)	22.39(0.02)	142.11(0.04)	283(-1)	4.6	249	0.35	0.23	0.27	0.33
10	May 25, 1979	1815:41.0(-0.2)	24.11(0.02)	142.27(0.01)	591(-2)	5.1	350	0.39	0.61	0.39	0.24
11	May 18, 1979	2018:03.5(0.0)	24.13(-0.00)	142.41(0.00)	599(1)	5.8	444	0.43	0.57	0.31	0.41
12	July 7, 1975	1928:44.3(-0.2)	25.97(0.03)	141.24(0.01)	139(-2)	5.5	293	0.70	0.72	0.30	0.38
13	Oct. 7, 1968	1920:20.8(0.0)	26.31(0.02)	140.71(0.01)	520(2)	6.0	378	0.31	0.27	0.02	0.30
14	March 15, 1978	2204:41.7(-0.1)	26.46(0.02)	140.77(0.01)	278(0)	5.9	452	0.51	0.48	0.17	0.38
15	Dec. 11, 1980	0157:47.0(-0.1)	26.51(0.03)	140.53(-0.04)	486(-5)	4.2	249	0.32	0.33	0.21	0.22
16	Feb. 14, 1976	1050:23.9(-0.1)	26.55(0.02)	140.32(0.01)	573(1)	5.4	368	0.40	0.59	0.13	0.25
17	Sept. 8, 1982	0237:32.8(-0.1)	26.99(0.05)	140.26(-0.02)	445(-5)	5.3	303	0.44	0.48	0.26	0.27
18	Jan. 15, 1973	0902:59.1(0.0)	27.08(0.03)	140.21(0.00)	488(2)	5.5	348	0.40	0.42	0.20	0.24
19	May 16, 1974	2000:03.3(0.2)	27.19(0.05)	140.16(-0.02)	490(1)	5.3	323	0.37	0.42	0.25	0.22
20	May 27, 1970	1205:08.1(-0.2)	27.24(0.02)	140.27(-0.02)	405(-1)	6.0	371	0.56	0.56	0.29	0.39
21	Nov. 13, 1972	0811:49.4(0.1)	27.95(0.03)	140.12(-0.01)	375(1)	5.5	244	0.35	0.39	0.11	0.22
22	April 16, 1980	0650:14.7(0.1)	28.00(0.03)	140.34(-0.02)	255(0)	4.2	352	0.41	0.52	-0.09	0.20
23	Dec. 12, 1976	0108:50.8(-0.3)	28.06(0.03)	139.64(-0.03)	500(-2)	5.8	460	0.31	0.51	0.23	0.23
24	Jan. 31, 1973	2055:54.0(-0.2)	28.24(0.03)	139.29(-0.00)	507(-1)	5.9	414	0.42	0.50	0.26	0.38
25	Jan. 17, 1980	0921:55.0(-0.2)	28.30(0.01)	138.88(-0.03)	520(-3)	4.2	309	0.25	0.57	0.09	0.18
26	May 13, 1977	1113:32.6(-0.3)	28.44(0.03)	139.57(-0.02)	446(-2)	5.6	495	0.35	0.39	0.14	0.32
27	Dec. 16, 1980	1308:25.4(0.1)	28.51(0.03)	139.76(-0.06)	399(-1)	4.5	301	0.50	0.54	0.20	0.37
28	Dec. 29, 1977	1945:28.5(0.0)	28.55(0.04)	138.51(-0.00)	541(0)	5.0	301	0.28	0.33	0.10	0.32
29	Oct. 23, 1967	0827:07.2(-0.1)	28.87(0.00)	139.26(-0.01)	477(2)	5.3	270	0.35	0.58	-0.10	0.23
30	Dec. 11, 1979	1726:18.3(-0.2)	28.97(0.02)	140.93(-0.01)	126(-1)	6.0	459	0.52	0.59	0.02	0.33
31	June 23, 1982	0151:55.5(0.0)	29.08(0.04)	138.83(-0.03)	483(-3)	5.1	335	0.19	0.44	0.07	0.11
32	Dec. 7, 1970	2135:21.6(-0.3)	29.81(0.02)	140.10(-0.01)	182(-1)	6.0	398	0.39	0.52	-0.06	0.25
33	June 25, 1976	0747:48.4(0.0)	29.92(0.03)	138.73(-0.01)	456(1)	5.4	330	0.29	0.29	0.07	0.29
34	Jan. 11, 1978	0810:14.2(0.0)	30.02(0.06)	138.85(-0.02)	428(-1)	5.1	249	0.29	0.35	0.36	0.15
35	Aug. 4, 1976	2321:45.4(0.0)	30.23(0.06)	138.61(-0.03)	444(-1)	5.4	359	0.18	0.39	-0.02	0.13
36	June 12, 1982	0602:02.8(-0.1)	30.36(0.01)	138.36(0.00)	459(1)	5.1	313	0.32	0.29	0.31	0.23
37	July 18, 1978	2158:19.2(0.0)	30.39(0.02)	137.26(-0.01)	503(2)	4.5	256	0.25	0.42	-0.08	0.22
38	March 4, 1971	0028:38.1(-0.2)	30.41(0.01)	138.44(0.00)	449(0)	5.5	314	0.35	0.35	0.08	0.37
39	April 20, 1977	2004:29.2(-0.1)	30.63(0.03)	137.61(-0.02)	493(-0)	5.5	438	0.17	0.28	0.02	0.15
40	March 6, 1967	0440:17.6(-0.3)	30.62(-0.02)	137.79(-0.03)	488(2)	5.0	245	0.21	0.27	-0.01	0.15
41	May 31, 1981	0842:18.6(0.1)	30.70(0.03)	137.70(-0.03)	482(1)	4.3	344	0.22	0.34	0.07	0.15
42	Nov. 29, 1974	2205:23.2(-0.3)	30.71(0.01)	138.40(-0.03)	428(-1)	6.0	421	0.36	0.23	0.09	0.41
43	June 26, 1975	0952:20.2(0.0)	31.85(0.01)	138.11(-0.03)	394(1)	5.3	307	0.18	0.45	0.07	0.02
44	March 7, 1978	0248:38.9(-0.2)	31.94(0.02)	137.60(-0.02)	436(0)	6.4	487	0.30	0.15	0.15	0.32
45	Aug. 12, 1975	1421:05.7(-0.2)	32.09(0.03)	137.86(-0.01)	399(-0)	5.5	444	0.44	0.33	0.26	0.45
46	Oct. 30, 1971	1416:23.2(-0.2)	32.09(0.00)	137.77(-0.03)	392(1)	5.5	338	0.34	0.35	0.20	0.33
47	March 5, 1981	1859:00.8(0.1)	32.13(0.02)	138.06(-0.03)	361(1)	4.8	291	0.35	0.42	0.20	0.25
48	April 22, 1980	0534:14.4(-0.1)	32.14(0.02)	137.69(-0.02)	402(1)	5.8	504	0.32	0.29	0.17	0.30
49	March 10, 1966	0426:21.1(-0.2)	32.29(-0.01)	137.70(-0.01)	399(2)	5.3	251	0.32	0.35	0.15	0.27
50	Oct. 12, 1979	0655:35.7(-0.1)	32.73(-0.01)	136.11(-0.04)	450(3)	4.2	255	0.24	0.20	0.17	0.28
51	June 24, 1974	1901:40.7(-0.1)	32.84(0.02)	137.07(-0.03)	402(1)	5.1	307	0.31	0.23	0.25	0.23
52	Jan. 6, 1981	1535:29.1(0.1)	32.97(0.03)	138.48(-0.03)	310(1)	4.4	319	0.35	0.38	0.28	0.22
53	Feb. 28, 1968	1208:01.6(-0.2)	32.96(0.01)	137.83(-0.02)	349(1)	5.5	351	0.22	0.42	0.06	0.05
54	May 29, 1975	1544:45.2(-0.1)	33.05(0.02)	137.21(-0.03)	386(1)	5.0	261	0.22	0.12	0.13	0.23
55	Oct. 29, 1972	0720:39.8(-0.1)	33.07(0.01)	137.91(-0.04)	346(1)	5.3	288	0.19	0.23	0.21	0.03
56	Feb. 22, 1974	0036:54.3(-0.3)	33.18(0.01)	136.95(-0.02)	391(0)	5.9	430	0.28	0.30	0.11	0.23
57	Sept. 27, 1978	1700:18.0(0.1)	33.57(0.03)	138.16(-0.05)	296(-0)	5.0	287	0.17	0.19	0.03	0.16
58	Nov. 10, 1970	0026:22.0(-0.2)	34.66(-0.01)	136.85(-0.01)	352(2)	5.1	278	0.23	0.27	0.13	0.17
59	Aug. 25, 1981	0656:24.3(0.0)	34.94(0.02)	136.82(-0.03)	335(2)	5.0	250	0.30	0.29	0.18	0.23
60	Aug. 13, 1967	2006:52.1(-0.2)	35.44(0.01)	135.47(-0.02)	369(2)	6.0	340	0.13	0.21	-0.09	0.12

TABLE 1. (continued)

Event	Date	Time, UT	Latitude °N	Longitude °E	Depth, km	m_b	n†	Correlation Coefficients‡			
								R_w	R_u	R_m	R_d
61	March 31, 1980	0732:32.3(-0.1)	35.52(0.03)	135.49(-0.03)	364(1)	5.4	473	0.29	0.20	0.22	0.25
62	Oct. 8, 1978	1909:22.2(0.1)	36.09(0.02)	137.25(-0.03)	255(2)	4.5	338	0.27	0.46	0.31	0.02
63	Dec. 29, 1976	1436:48.8(-0.2)	36.73(0.02)	139.10(-0.04)	142(1)	5.3	369	0.35	0.40	0.12	0.30
64	Feb. 3, 1982	2042:45.2(-0.1)	36.91(-0.00)	135.67(-0.02)	346(1)	5.3	454	0.23	0.32	0.13	0.20
65	Aug. 29, 1970	0143:12.2(-0.1)	37.00(-0.00)	136.81(-0.00)	287(2)	5.1	272	0.18	0.33	0.19	0.07
66	Sept. 21, 1971	0843:31.9(-0.0)	37.36(0.02)	138.69(-0.03)	188(2)	5.4	252	0.28	0.40	0.14	0.16
67	May 28, 1979	1439:35.0(0.0)	37.42(0.01)	136.81(-0.04)	282(2)	5.0	320	0.18	0.36	0.20	0.04
68	June 21, 1980	2130:17.7(-0.1)	37.43(0.01)	134.98(-0.02)	372(2)	5.0	333	0.26	0.27	0.16	0.17
69	Jan. 18, 1980	2210:15.1(-0.1)	37.87(0.02)	133.41(-0.02)	427(2)	5.4	463	0.40	0.21	0.04	0.51
70	March 6, 1978	1511:38.2(-0.1)	38.34(0.02)	133.99(-0.01)	416(2)	5.0	316	0.25	0.20	0.13	0.24
71	March 31, 1969	1925:26.7(-0.3)	38.49(0.00)	134.51(-0.01)	397(0)	5.6	325	0.21	0.08	-0.02	0.28
72	June 29, 1975	1037:40.4(-0.2)	38.79(0.01)	130.10(0.01)	550(1)	6.0	485	0.45	0.50	0.30	0.39
73	March 23, 1970	0020:54.7(-0.4)	40.18(0.00)	140.30(-0.01)	146(-1)	5.5	284	0.28	0.22	0.13	0.28
74	Sept. 5, 1973	0030:53.8(-0.1)	40.70(0.02)	139.62(-0.01)	194(1)	5.5	299	0.13	0.08	0.12	0.13
75	June 9, 1980	2006:35.1(0.0)	40.87(0.03)	139.95(-0.02)	169(2)	5.6	413	0.29	0.26	0.20	0.28
76	June 10, 1971	1959:53.0(-0.3)	41.08(-0.01)	138.48(-0.03)	234(1)	5.5	345	0.31	0.32	0.16	0.30
77	Nov. 23, 1975	2302:08.2(0.1)	41.28(0.03)	140.16(-0.04)	170(3)	5.3	253	0.18	0.18	0.11	0.22
78	Oct. 21, 1978	0236:10.1(-0.1)	41.27(0.01)	135.55(0.01)	362(0)	5.0	281	0.14	0.22	0.07	0.06
79	Feb. 2, 1967	1624:39.7(0.0)	41.60(0.04)	139.83(-0.01)	185(3)	5.3	259	0.25	0.25	0.16	0.22
80	July 28, 1981	1700:57.6(-0.1)	41.66(0.01)	140.03(-0.01)	181(1)	5.4	431	0.38	0.41	0.24	0.31
81	March 9, 1977	1427:56.0(-0.2)	41.69(0.03)	131.05(0.00)	559(3)	5.9	564	0.31	0.61	0.33	0.13
82	Aug. 16, 1979	2131:24.6(-0.3)	41.86(0.01)	130.87(0.01)	565(-1)	6.0	555	0.39	0.53	0.35	0.32
83*	Sept. 29, 1973	0044:00.2(-0.1)	41.96(0.03)	130.96(-0.02)	571(4)	6.3	460	0.38	0.56	0.35	0.25
84	April 10, 1969	1454:03.6(-0.1)	42.12(0.02)	131.06(-0.00)	551(4)	5.1	248	0.40	0.42	0.45	0.26
85*	Sept. 10, 1973	0743:32.0(-0.3)	42.48(-0.00)	131.01(-0.04)	554(2)	5.8	446	0.26	0.49	0.31	0.12
86	Nov. 8, 1974	2123:22.1(-0.1)	42.54(0.01)	141.70(-0.04)	127(1)	5.9	436	0.34	0.17	0.15	0.37
87	Aug. 17, 1969	1154:55.0(-0.1)	42.67(0.03)	141.43(-0.04)	135(2)	5.5	291	0.40	0.36	0.25	0.38
88	Jan. 31, 1979	1236:24.0(-0.2)	42.78(-0.00)	131.20(-0.00)	537(2)	4.8	432	0.35	0.36	0.34	0.20
89	April 11, 1976	1303:36.6(-0.2)	42.82(0.02)	131.07(0.02)	542(1)	5.0	250	0.36	0.40	0.36	0.23
90	Nov. 27, 1981	1721:44.1(-0.2)	42.95(0.02)	131.19(0.01)	526(2)	5.6	558	0.42	0.40	0.43	0.28
91	Aug. 20, 1966	0932:31.5(0.0)	43.03(0.05)	140.56(-0.04)	165(3)	5.5	248	0.34	0.16	0.23	0.34
92	July 4, 1967	2342:12.7(-0.2)	43.12(0.02)	142.55(-0.03)	159(2)	5.5	303	0.29	0.24	0.12	0.24
93	Dec. 25, 1979	0336:52.0(-0.3)	43.26(0.03)	131.27(0.02)	522(-2)	4.9	281	0.37	0.24	0.35	0.32
94	June 15, 1978	0319:08.9(-0.1)	43.42(0.02)	135.41(-0.03)	369(4)	4.8	358	0.32	0.39	0.08	0.24
95	May 6, 1973	1439:27.2(-0.1)	43.55(0.01)	132.35(-0.01)	488(3)	5.1	316	0.30	0.40	0.15	0.19
96	Feb 28, 1966	0202:12.7(-0.2)	43.71(0.02)	139.65(-0.02)	220(2)	5.5	256	0.28	0.34	0.12	0.26
97	June 21, 1979	1405:45.5(-0.3)	43.77(0.01)	139.75(-0.00)	216(-1)	4.3	347	0.41	0.36	0.34	0.39
98	Aug. 6, 1975	2137:39.8(0.0)	43.94(0.04)	139.34(0.01)	231(1)	5.5	305	0.29	0.28	0.29	0.29
99	Oct. 25, 1965	2234:22.2(-0.2)	44.21(-0.00)	145.44(-0.01)	160(1)	6.0	342	0.39	0.23	0.25	0.46
100	May 31, 1981	2359:34.0(-0.3)	44.49(0.00)	137.31(-0.01)	288(1)	5.5	406	0.39	0.35	0.12	0.49
101	Jan. 19, 1969	0702:07.4(-0.5)	44.89(-0.00)	143.21(0.00)	237(-1)	6.3	397	0.32	0.18	0.09	0.37
102	April 9, 1974	1311:23.5(-0.1)	45.42(0.04)	148.39(-0.02)	160(1)	5.4	253	0.23	0.26	-0.16	0.25
103	July 14, 1982	1042:12.6(0.0)	45.78(0.05)	143.25(-0.02)	314(3)	5.1	315	0.17	0.21	0.21	0.09
104	Jan. 29, 1978	0205:01.3(-0.1)	45.85(0.01)	149.22(0.02)	151(1)	5.0	271	0.35	0.35	0.10	0.35
105	March 29, 1976	1948:39.1(-0.6)	45.97(0.01)	149.50(-0.00)	159(-4)	5.4	243	0.34	0.35	0.18	0.20
106	Dec. 27, 1972	1406:07.2(-0.2)	46.18(0.01)	144.04(0.01)	328(2)	5.1	324	0.33	0.32	0.18	0.31
107	Dec. 18, 1969	1332:04.0(0.1)	46.25(0.04)	142.44(-0.01)	334(5)	5.9	352	0.32	0.16	0.07	0.39
108	Nov. 11, 1975	0425:32.1(-0.2)	46.72(0.00)	145.47(0.01)	351(1)	5.4	313	0.28	0.48	0.13	0.18
109	June 13, 1973	0020:52.2(-0.6)	46.91(0.01)	151.05(0.00)	173(-2)	5.4	275	0.28	0.25	0.03	0.24
110	June 19, 1977	1147:23.5(-0.4)	47.14(0.02)	151.09(0.01)	154(-1)	5.5	401	0.32	0.36	0.06	0.23
111*	July 10, 1976	1137:13.9(-0.1)	47.33(0.03)	145.75(-0.00)	404(3)	5.8	451	0.21	0.21	0.26	0.13
112	July 20, 1979	2120:01.6(-0.9)	47.40(0.00)	152.35(0.00)	129(-6)	4.2	241	0.24	0.21	0.24	0.17
113	Dec. 11, 1980	2253:24.2(-0.3)	47.82(0.04)	146.08(0.01)	436(-1)	5.0	252	0.23	0.04	-0.04	0.37
114	Nov. 22, 1966	0629:51.9(-0.5)	48.00(-0.00)	146.78(-0.01)	441(-2)	5.5	277	0.30	0.27	0.11	0.23
115	March 25, 1972	0056:03.0(-0.9)	48.03(-0.00)	153.11(-0.01)	119(-4)	5.8	304	0.24	0.42	0.10	0.08
116	Dec. 22, 1980	2031:43.7(-0.3)	48.21(0.03)	146.23(-0.00)	465(-0)	5.3	359	0.22	0.22	0.11	0.25
117	March 3, 1971	2154:08.9(-0.8)	48.25(0.02)	153.09(0.02)	123(-4)	5.6	270	0.21	0.35	0.04	0.12
118*	June 21, 1978	1110:38.3(-0.4)	48.28(0.01)	148.64(-0.02)	379(-1)	5.8	506	0.25	0.14	0.19	0.26
119	Feb. 6, 1981	1647:08.2(-0.3)	48.29(0.01)	146.39(0.01)	490(0)	4.7	460	0.23	0.14	0.11	0.25
120	March 11, 1974	1137:30.8(-0.8)	48.31(0.01)	153.16(0.00)	149(-5)	5.8	348	0.31	0.33	0.16	0.22

TABLE 1. (continued)

Event	Date	Time, UT	Latitude °N	Longitude °E	Depth, km	m_b	n†	Correlation Coefficients‡			
								R_w	R_s	R_m	R_d
121	Oct. 14, 1972	0000:22.8(-0.2)	48.35(0.02)	148.77(0.00)	375(-0)	5.5	262	0.29	0.29	0.17	0.23
122	Dec. 20, 1977	0850:37.9(-1.5)	48.59(0.03)	153.07(0.01)	141(-12)	5.6	328	0.19	0.28	0.06	0.05
123*	March 22, 1972	1027:41.0(-1.1)	49.00(-0.05)	153.61(0.02)	128(-7)	6.1	349	0.39	0.34	0.26	0.22
124	Jan. 29, 1982	0002:04.2(-0.3)	49.17(0.02)	147.88(0.00)	532(-0)	5.0	337	0.37	0.44	0.16	0.18
125	Dec. 1, 1967	1357:02.6(-0.8)	49.48(0.03)	154.41(0.01)	139(-5)	5.9	308	0.14	0.13	0.09	0.07
126*	Aug. 21, 1972	0623:48.0(-0.6)	49.48(0.01)	147.07(0.00)	570(-4)	5.9	338	0.20	0.34	0.14	0.09
127	Dec. 20, 1974	1638:55.0(-0.3)	49.75(-0.00)	149.75(0.01)	411(-1)	5.0	263	0.37	0.44	0.21	0.27
128	May 12, 1977	2137:33.1(-0.5)	50.10(-0.01)	155.04(0.01)	128(-2)	5.1	301	0.24	0.09	0.31	0.16
129	March 6, 1972	1850:16.0(-0.8)	50.15(0.02)	148.79(-0.01)	563(-7)	5.4	250	0.30	0.39	0.18	0.19
130	Nov. 27, 1982	0955:38.6(-0.3)	50.23(0.04)	147.75(-0.01)	618(-1)	5.5	466	0.29	0.54	0.11	0.12
131	Oct. 28, 1978	1630:17.8(-0.7)	50.23(-0.00)	155.73(0.02)	133(-5)	4.6	244	0.46	0.37	0.31	0.29
132*	July 28, 1973	2006:35.0(-0.4)	50.47(0.03)	148.91(-0.01)	583(-2)	5.5	312	0.27	0.38	0.21	0.12
133	Jan. 25, 1979	2103:20.4(-0.5)	50.48(0.02)	148.92(.01)	569(-4)	4.3	339	0.23	0.28	0.14	0.11
134	Aug. 8, 1982	0614:07.4(-2.0)	51.07(0.03)	156.41(0.00)	122(-17)	5.0	255	0.36	0.30	0.30	0.12
135	Oct. 13, 1981	1553:55.4(-1.2)	51.44(-0.00)	157.43(0.02)	113(-9)	5.3	245	0.27	0.25	0.12	0.16
136	June 10, 1980	2313:23.7(-0.4)	51.53(0.02)	150.63(-0.01)	545(-3)	4.5	306	0.18	0.34	0.22	0.07
137*	Jan. 29, 1971	2158:02.3(-0.9)	51.69(-0.00)	150.99(0.02)	508(-7)	6.0	356	0.21	0.27	0.17	0.09
138*	Sept. 21, 1977	2101:43.5(-0.9)	51.72(0.02)	155.26(0.03)	230(-6)	5.5	411	0.23	0.19	0.23	0.13
139*	June 26, 1972	1005:59.4(-0.9)	51.88(0.01)	156.14(0.01)	187(-10)	5.4	288	0.36	0.42	0.26	0.17
140*	Dec. 21, 1975	1054:16.6(-0.6)	51.93(0.01)	151.56(-0.01)	543(-3)	6.0	428	0.33	0.79	0.21	0.11
141	Oct. 12, 1967	1253:45.4(-0.5)	52.16(0.01)	152.57(0.00)	464(-2)	5.5	243	0.33	0.48	0.24	0.26
142*	Aug. 22, 1979	1828:53.1(-1.8)	52.23(0.01)	157.35(0.02)	116(-13)	5.0	348	0.33	0.44	0.13	0.18
143*	Sept. 5, 1970	0752:26.6(-0.6)	52.27(-0.01)	151.49(0.00)	558(-2)	5.6	330	0.31	0.44	0.14	0.30
144*	Aug. 30, 1970	1746:08.2(-0.7)	52.36(0.00)	151.64(-0.00)	639(-4)	6.5	384	0.11	0.53	0.23	0.04
145	Dec. 30, 1979	418:31.6(-0.5)	52.53(0.02)	152.30(0.01)	527(-4)	4.8	338	0.36	0.38	0.17	0.29
avg.	—	—	—	—	—	—	336	0.30	0.34	0.17	0.23

Values in paratheses correspond to new source location values minus ISC values.

† n number of receivers used.

‡ Correlation coefficient between residuals of the observed and predicted, both are unsmoothed: R_w, predictions are from the whole mantle model; R_s, predictions are from the upper mantle model; R_m, predictions are from the middle mantle model; R_d, predictions are from the deep mantle model.

* Event which has been analyzed by *Creager* and *Jordan* [1984, 1986].

Hence the four unknowns $\delta t°$, $\delta\theta$, $\delta\phi$, and δh in the equation can be solved iteratively in a linear least square sense. Figure 2 provides one example showing the effect of source mislocation on a residual sphere by perturbing a relocated hypocenter 0.1° laterally and 10 km in depth. Notice that all perturbed hypocenters result in higher residual variances than that of the unperturbed, indicating that the hypocenter is relocated properly The observed residual spheres of events 83, 126 and 137 (in Figures 9, 12 and 14 shown later) are very similar to those of the same events of *Creager and Jordan* [1984], even though the data are corrected in different ways We hence conclude that our differing conclusions are not due to different patterns in the data or different source location biases.

The P wave velocity models utilized are obtained from iterative inversions of ISC travel time data. The first is a global mantle P wave velocity model of block size 5°×5°×100 km [*Clayton and Comer*, 1983, *Hager and Clayton*, 1989], which is based on ISC travel time delays at epicentral distance greater than 25°. The second is a regional P wave velocity model of block size 2°×2°×50 km [*Zhou and Clayton*, 1987, 1990], which is based on regional ISC travel time delays that cover the upper mantle and upper portion of the lower mantle around the subduction zones of the northwest Pacific. Analyses of resolution and noise show that the images are generally resolved well [*Zhou*, 1988]. The top portion of the regional model contains coherent high-velocity heterogeneities associated with Wadati-Benioff seismicity zones. These fast velocities, interpreted as the signature of the subducted lithosphere, are slablike in the shallow mantle but, in many places, tend to be contorted and flattened as they deepen. In general, the expected correlation of seismic activity and fast, assumably cold, mantle features is confirmed.

We have constructed a composite mantle velocity model by embedding the regional model into the global model, excluding regions in the global model that overlap with the regional model. Variants of the composite model are used to predict travel time residuals The first variant is the entire composite model, or the whole mantle model. The second variant is the near-source upper mantle model, the upper mantle portion (<650 km) of the regional model. The third variant includes the region between 650 and 1500 km beneath the source area, the range of interest for the

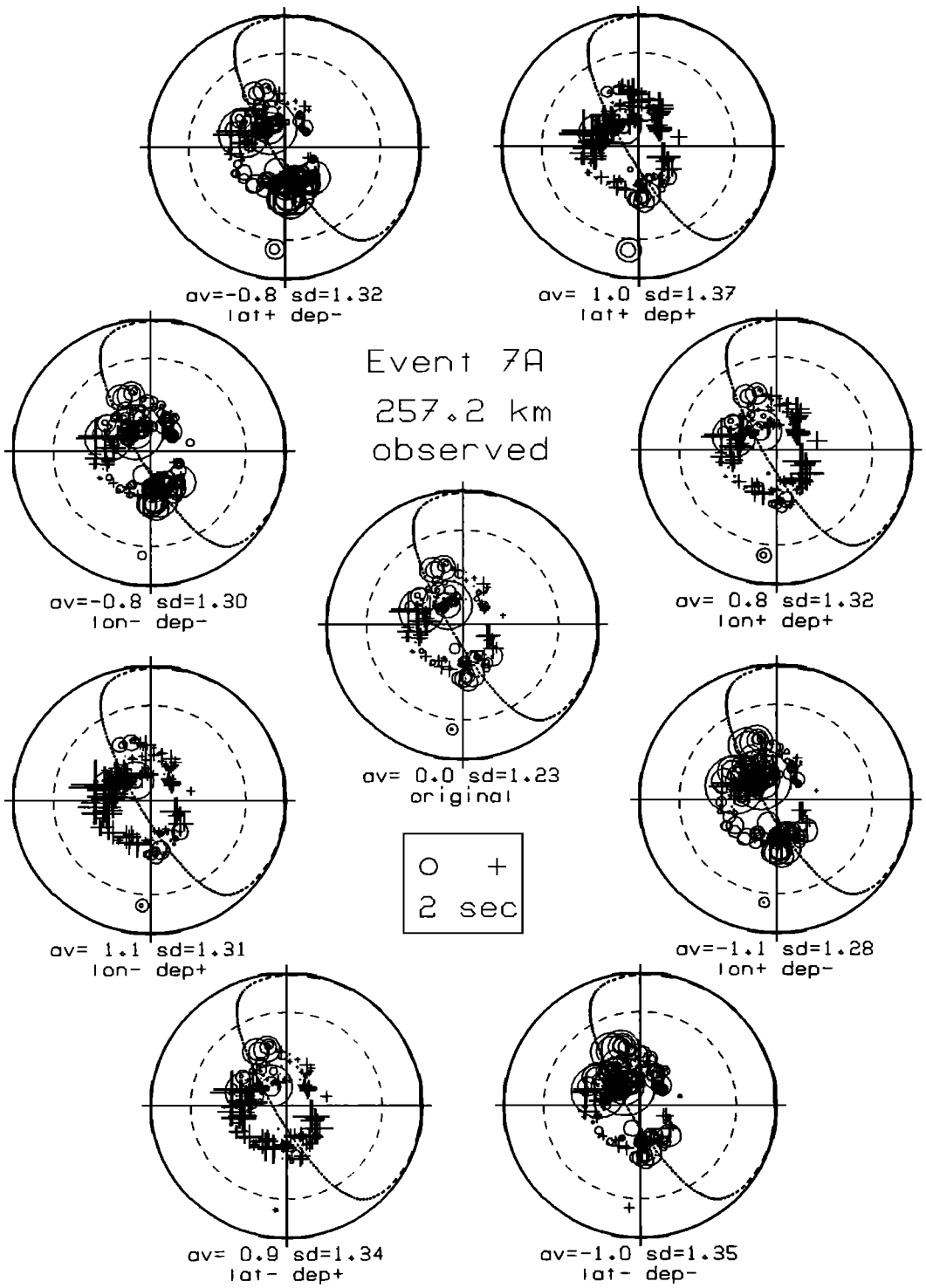

Fig. 2. Effect of source mislocation on residual sphere anomalies. All residual spheres shown here are for observed residuals of event 7. The center one is at the relocated location, while the hypocenters of eight surrounding spheres are perturbed (+ and -) 0.1° laterally and 10 km in depth from the relocated location. On each residual sphere, crosses and circles denote late and early arrivals, respectively, and their sizes correspond to the magnitudes. The light dashed circle represents 90° (horizontal) takeoff angle, and residuals inside and outside correspond to downgoing and upgoing rays, respectively. The circumference corresponds to rays that go vertically up. The heavy dashed curve indicates the slab orientation from seismicity. Notice that the standard deviation of residuals is a minimum at the relocated hypocenter, and most residual sphere features are robust with the given amount of hypocenter perturbation. For example, open circles tend to lie along the trend of the slab in all the residual spheres.

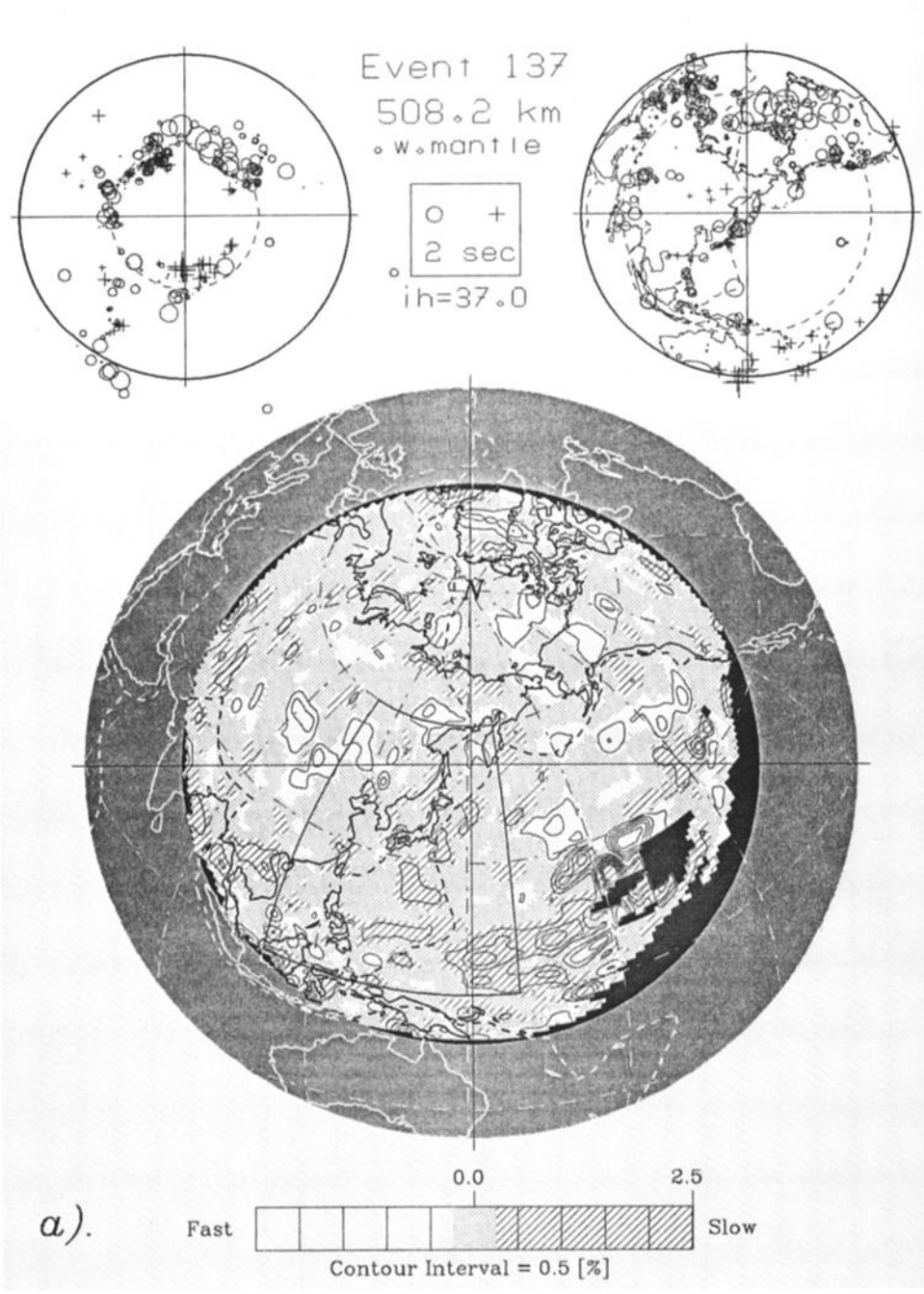

Fig. 3. Effect of mantle velocities on computed residual sphere of event 137. The large circle map, which shows coast lines and plate boundaries, is centered on event 137 in the Kuriles. The superimposed pattern is a projection (Figure 4) of the seismic velocity on a surface swept out by an initial cone of rays with a constant takeoff angle (37° for Figure 3*a* and 28° for Figure 3*b*) from the source at the center. The rays are diving into the mantle in the inner part of the circle and are rising toward the surface in the outer part of the map. The surface of Earth is in grey, while the unsampled mantle regions are in black. The fast and slow regions are contoured and patterned (stipples are slow; whites are fast; and grey tones are within a quarter percent of the layer mean). The location of the regional model is outlined. The ray-surfacing points are indicated by a dashed circle in the two smaller circle plots on the top, the standard residual sphere on the left, and the station location residual map

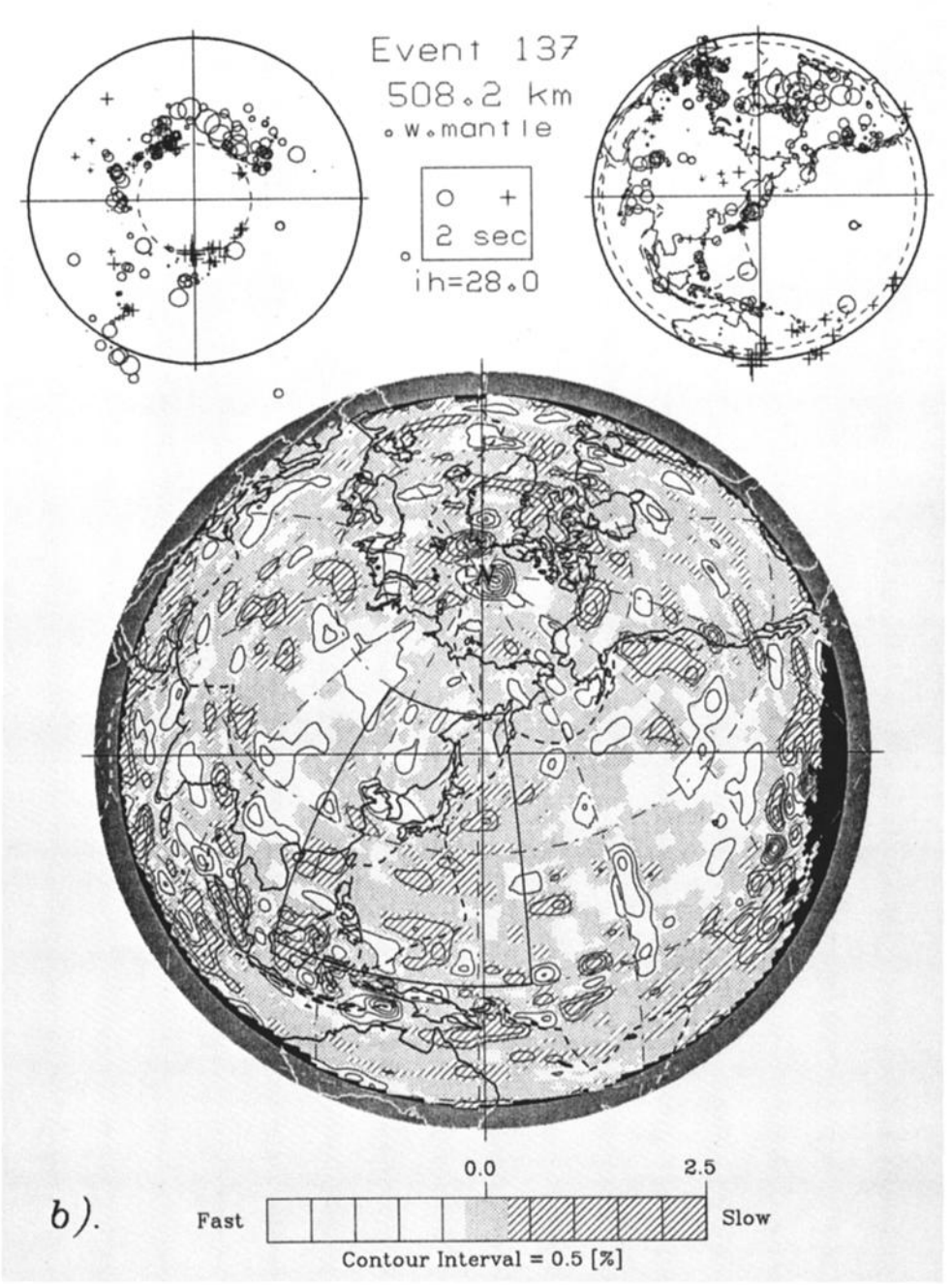

Fig. 3. (continued)

on the right. The legend of the residual sphere follows that of Figure 2, except that the circumference here corresponds to takeoff angle of 90°. The station location residual map has the same map orientation as that of the velocity map but with computed travel time residual plotted at each station location. Opposite to the sense of distance for the station location residual map, the radial direction on the residual sphere is takeoff angle. The ray-bottoming depths are about 1810 km for Figure 3*a* and 2550 km for Figure 3*b*. Long-wavelength velocity variations are visible in both plots. Note in Figure 3*a* that velocities are generally fast in the NE quadrant and slow in southern directions. The velocity map is applicable only to stations located close to the ray-surfacing circle; i.e., the magnitude of travel time residual for such a station is an integral along a straight line connecting the origin and the station.

deep slab penetration hypothesis. The fourth variant is the first variant (whole mantle model) minus the second (near-source upper mantle) and third variants (near-source middle mantle). This should be free of any effect caused by the subduction zones of the northwest Pacific, because at 1500 km depth the rays have spread out and narrow slablike features will not show up as coherent patterns affecting more than a few stations. We refer to the second, third, and fourth variants as the upper mantle, middle mantle, and deep mantle models and to their combination, the first variant, as the whole mantle model. Notice that the "deep mantle" model actually also includes upper mantle and middle mantle regions outside the area of the regional velocity model; these regions are traversed by the upgoing legs of teleseismic rays. By examining predicted residual spheres from each model, the locations of the velocity heterogeneities that contribute to the calculated residual sphere anomalies are isolated in the models. The similar patterns in the observed and predicated residual spheres are then suggestive of the locations of real mantle heterogeneities. A shortcoming of the residual sphere method is that ordinarily there is no constraint on the locations and magnitudes of the anomalies. The deep slab penetration hypothesis, for example, is based on assumptions about both the location and the magnitude of the mantle anomaly that causes a given residual sphere anomaly.

Being based on tomographic inversions of seismic data the velocity models used differ considerably from the simple idealized slab models used in previous studies. Of course, these models contain noise due to data error, poor ray coverage, and limited resolution of the inversion We do not intend to discuss the derivation of the velocity models themselves nor do we argue that they are well enough known to be removed from the data in order to discuss residual near-source effects. At the very least, these models can be viewed as independently determined structures which introduce "noise" into residual spheres, complicating the use of this kind of data for near-source studies of slab structure At the other extreme, if the velocity models predict the observed residual sphere data well, then one cannot rule out the possibility that some aspects of the models are real The residual sphere modeling process certainly provides a different viewpoint for evaluating three-dimensional velocity models

3. MODELING OF RESIDUAL SPHERES

The main topic of this paper is the comparison of observed residual focal spheres with those obtained by tracing rays through each of the four regional variants of velocity models, hence to determine the contribution to the residual sphere from the various mantle sources. The geometry of the computed ray paths is controlled by the JB model. From this point on the figure captions are an important part of the text and much of the discussion is not repeated in the text.

Figure 3 illustrates the effect of heterogeneities at various mantle locations on the residual sphere patterns. It is a special projection (Figure 4) of the composite velocity model along a set of "conical" ray paths of a constant takeoff angle (ray parameter). The average velocity of each layer (shell)

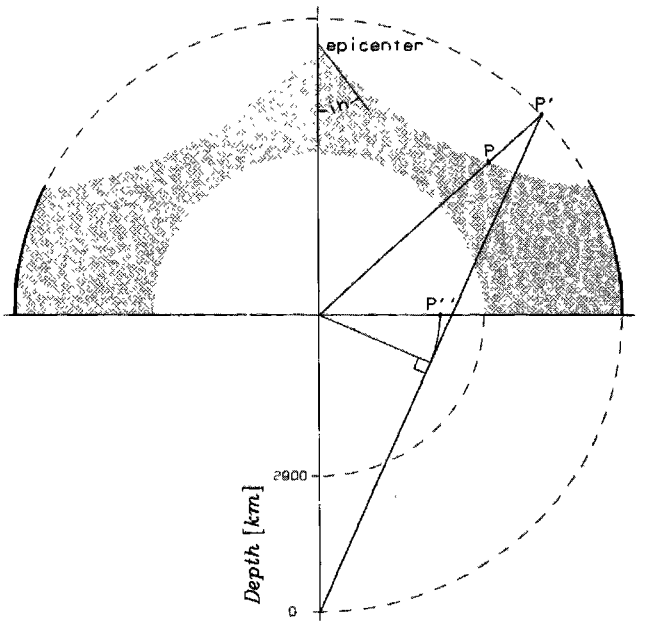

Fig. 4. The projection of velocity map in Figure 3. This is a cross section view of the velocity map in Figure 3*a*. The mantle velocity anomaly at a point P, which is traversed by a ray at the constant takeoff angle (ih) from the hypocenter, is taken to a surface point P' and then projected to a point P'' on the velocity map. In this way, the mantle velocities that are traversed by a cone of rays of a given takeoff angle are mapped Note that the locations of the traversed points depend on the source location and the given takeoff angle. The maps are equal-area projections.

has been removed. The large-scale spatial variation of velocity is clearly evident. Note the fast and slow anomalies in the middle lower mantle (Figure 3*a*) and in the bottom lower mantle (Figure 3*b*). Many anomalies are of large-scale and far from the source region (the center of the map). The calculated residual sphere pattern can be directly related to certain mantle heterogeneities. A residual at a station located close to the dashed circle is generated by the heterogeneities, shown in the velocity map, along a straight line connecting the station with the center of the map (the source). Notice that the teleseismic arrivals from this Kuril event are affected by deep lower mantle velocity variations that are relatively fast along the strike direction of the Kuril trench. In fact, one of the reasons for showing the velocity maps of this event is that the regional velocity model has deep, probably slab-related, fast "fingers" beneath the Kuril trench. These are the small fast features near the center of the maps. Even in this case, however, the contribution to the residual sphere from these fast slablike features is less than from other fast regions which have no clear connection with the northwest Pacific subduction zone.

Lower mantle models from other studies, summarized by *Dziewonski and Woodhouse* [1987], also show a broad band of fast velocities from eastern North America to Southeast Asia, i.e., along strike of the Northwest Pacific subduction zones The long-wavelength velocity variations in the deep mantle mean that residual sphere travel time anomalies

may accumulate rather than cancel. If lower mantle effects do not cancel, a basic premise of residual sphere interpretations concerning deep slab penetration is invalid.

For the purpose of examining steep slabs, previous residual sphere studies [e.g., *Creager and Jordan*, 1984] used narrow cones (±60° takeoff angles minus core phases) of downgoing rays The cosine taper adopted in their smoothing operator (equation (23) of their paper) diminishes higher takeoff angle travel time residuals. Shallow dipping structures or horizontal high-velocity slabs (e.g., see discussion for event 83 later) hence would not be detected in these studies. Previous studies would interpret any large coherent structure in the deep mantle as a steeply dipping near-source structure. The focus of this paper is on the comparison of the predicted and observed residual sphere patterns and identification of the responsible (model) mantle heterogeneities. Consequently, residuals from the entire focal sphere, except core phases, are included in the comparison As expected, the upper residual sphere, which samples the slab above the earthquake, exhibits a slablike pattern for most of the events in this study

We use a spherical harmonic fitting to smooth the residual sphere data so that we can more directly compare our results with those of *Creager and Jordan* [1984, 1986]. These authors compared only smoothed versions of data and prediction. Their smoothing scheme, which is rather complex with ad hoc adjustable parameters, has a mean filter half width of 42° [*Creager and Jordan*, 1984], which corresponds closely to spherical harmonics of degree 3 (half width 45°). Our smoothing, using spherical harmonics of degree 0-6, is objective and simple. As mentioned earlier, however, the individual harmonic coefficients obtained in the fitting are aliased due to uneven and low station coverage; hence the only reason for the fitting is to provide smoothed versions of residual sphere anomalies.

Our unsmoothed data generally agree with that presented by *Creager and Jordan*'s [1984] (see their paper and Figures 9, 12, and 14 later in this paper). Our smoothed results are similar, for the most part, to the published results of Creager and Jordan, although they used a much heavier (lower-pass) smoothing which yields an almost perfect match between data and model for every event. It is generally true that a heavier smoothing on both the data and model results in a better match, but the sense of "data" is correspondingly lost. Our spherical harmonic smoothing of degree 0-6 has raised the correlation substantially (see Figures 5-15). The identical cosine taper, equivalent to a degree one weighting, applied by Creager and Jordan to both data and model calculations also tends to force agreement between the two as well as to eliminate shallow dipping structures from further analysis. Since the effect of smoothing is so strong, we perhaps should not concentrate on comparing data and prediction after heavy smoothing but try to determine what is affecting the unsmoothed data. Consequently, the major task of this paper is simply on comparing the predictions of various regions of the mantle model with the observed data

Some example residual spheres of the data and predictions, along with corresponding smoothed versions are shown in Figures 5-15. The correlation coefficient r between observed data and each prediction is also given in these figures. When a portion of a model contains gaps, i.e., regions that are poorly covered by crossing rays and regions exterior to the model, those rays that traverse entirely in gaps of a model are excluded from the correlation computation. The correlation coefficients for raw data residual spheres of each event (prior to spherical harmonic smoothing) are listed in Table 1. The correlation between the observed data and the whole mantle model predictions for all events exceed the 99% confidence level (most meaningful for the unsmoothed version) as determined from a Student's t test [e.g., *O'Connell*, 1971] As described in detail in the figure captions, the observed and predicted residual spheres are similar in pattern and general characteristics, and both have long-wavelength as well as short-wavelength variations Surprisingly, some of the short-wavelength anomalies are caused by near-source heterogeneities. These are particularly evident as rapid changes in sign. See, for example, the computed residual spheres for the middle mantle for most events. For most residual spheres, the amplitudes of the predicted anomalies from the whole mantle model are about the same as the amplitudes of the observed anomalies.

Creager and Jordan [1984] showed that Sea of Okhotsk earthquakes deeper than 400 km are dominated by NE-SW trending troughs of negative anomalies (i.e., fast arrival times) having strikes and dips similar to the seismic zone and having P wave anomalies of 1-2 s We have found similar trends in the present study. Creager and Jordan interpret their results in terms of slab penetration to depths of at least 900-1000 km, implying circulation of at least some upper mantle material into the deep mantle. We found, however, that independently derived lower mantle models, when projected onto the residual sphere, give similar fast bands caused primarily by heterogeneities exterior to that part of the mantle between 650 and 1500 km beneath the earthquakes. Examples of diffuse deep mantle structure having the trends of NW Pacific subduction zones are also evident in the study of *Dziewonski and Woodhouse* [1987].

Event 83 is the same as event 8 of *Creager and Jordan* [1986]. Notice the similarity in residual sphere patterns for steep rays (near the center of plot) in our smoothed data and whole mantle prediction with the smoothed data presentation by Creager and Jordan. The main features here are fast arrivals to the NW and slow anomalies to the west, NE and SE. These features are also evident in the predictions of the "deep mantle" model (lower panel). Many of the other features of the data (top panel) are caused by variations in the upper mantle (middle panel). The mantle between 650 to 1500 km depth (on the downgoing ray), however, predict a fast feature with nearly zero dip which has less amplitude and structure, in comparison with the deep mantle. It indicates flattening of the slab below about 571 km depth. The fast arrivals in the data which are unexplained by the upper and deep mantle models are not on the trend of the seismic zone and therefore provide little support for the slab penetration hypothesis.

Figure 12 shows results for event 126 in the Sea of Okhotsk. This is the same as event 6 of *Creager and Jordan* [1984] and event 7 of *Creager and Jordan* [1986], which they used as the main evidence for their deep slab penetration hypothesis. A cluster of fast arrivals along the seismicity trend in the N-NE directions is evident in both our

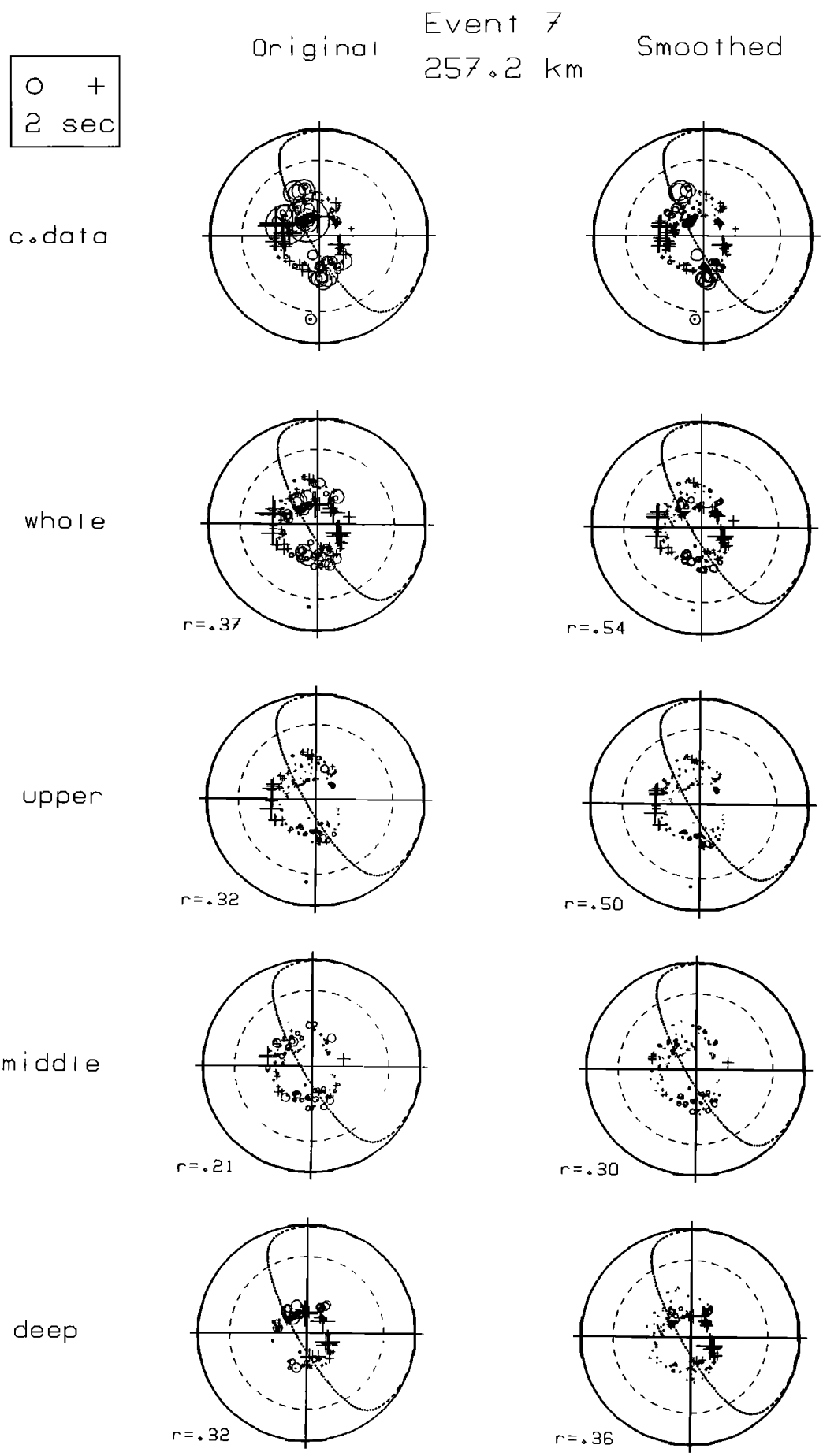
Event 7
257.2 km
Original
Smoothed
O +
2 sec
c.data
whole
r=.37
r=.54
upper
r=.32
r=.50
middle
r=.21
r=.30
deep
r=.32
r=.36

smoothed version of deep mantle prediction and the plot by these authors. This suggests that the anomaly is due to a diffuse high-velocity region in the deep mantle. In fact, the rays contributing to this band are widely spread out by the time they reach 1500 km depth.

Event 137 (Figure 14), a 508-km-deep event in the Kuril region, is the same as *Creager and Jordan*'s [1986] event 6. This gives another opportunity to compare the different smoothing and event location procedures This event is about 150 km above the normal boundary between the upper and lower mantles. The boundary, however, is possibly much deeper beneath cold slabs. The common features are a band of fast arrivals along but steeper than the trend of the seismic zone and slow arrivals to the NW, east and south. The total range of the data (in the region where coverage is common) is about 2-3 s. This is an important test because a serious error in event location would change the pattern and amplitude of observed residual spheres. Although they used different smoothing and location procedures, the observations shown by *Creager and Jordan* [1986] generally agree well with ours. They interpreted the patches of fast residuals as being due to a fast slab, beneath the event, indicating "slab penetration to depths exceeding 1000 km." Our results, however, show that much of the residual is accumulated by rays that have spread out into the deep lower mantle. The "deep" mantle (from 1500 km depth below the source to the receiver) contributes fast arrivals in the N-NE and SW directions, and the upper and middle mantles contributes slow arrivals to the NW. Note that the upper mantle also gives some fine structures, e.g., a slow patch to the SW surrounded by fast patches. The middle mantle which is relevant to the deep slab penetration hypothesis, 650-1500 km depth interval beneath the source, contributes a minor part to the overall residual sphere prediction.

4. A TEST FOR DEEP MANTLE VELOCITY HETEROGENEITY

We have arrived at an important conclusion in the previous section; that is, the deep mantle alone, far below the postulated depth of slab penetration and deep enough so that the seismic ray bundles are spread far beyond the confines of narrow slabs, predicts residual spheres having the general patterns of observed residual sphere data for deep focus earthquakes. Of course, this result is based on the velocity models used. We now design a very simple test, using only observed travel time residuals without any velocity models.

In this test, we first take all events that were recorded by a large number (>400) of receivers. The 33 events thus selected are well spread over the NW Pacific region (see solid stars in Figure 1) where the subduction zone is highly variable in strike and in dip. We then calculate the average residual at each teleseismic station that has picked up more than 16 of these events. The variability of the slab trend means more cancellation for the near-source effects, hence relatively more power for deep mantle and receiver effects In this procedure the rays from the various sources only sample similar mantle after they have travelled some distance from the source. The rays converge as they travel. The new station residual averages from the selected events represent a cumulative contribution from mantle regions far away from the source region, comparable to a true deep mantle model We finally take the mean location of the selected events as a hypothetical hypocenter to construct a residual sphere (Figure 16*a*) using these new station residual averages.

If the deep mantle anomalies are unimportant or not coherent over large distances, the residual sphere produced in this test should have a very small amplitude and a random pattern. However, as we can see in Figure 16, this is surely not the case. The station residual averages are around 1 s in magnitude (peak-to-peak well above 2 s) and form very distinctive patterns which correlate with major tectonic features. The large fast averages at stations in New Guinea and Timor Islands are likely due to upper mantle effects of the major Sunda subduction zones. On the other hand, large slow residual averages at the island stations of Marquesas, Tahiti, and Cook Islands are probably due to deep slow mantle beneath the west Pacific. The Canadian, Australian, and Baltic shields are fast. Western North America and central Asia are also very evident as slow anomalies. Variations of the event selection criteria for the above test do not change the result qualitatively. Remember that our previous data corrections include a removal of the station residual averages of *Clayton and Comer* [1983] which are based on a global data base. The above result therefore suggests that a global average of

Fig. 5. Residual spheres of event 7. The format of each residual focal sphere is the same as described in the caption of Figure 2. As indicated to the left, the top pair of residual spheres is the observed, followed (downward) by four pairs of predictions from four mantle models. The left and right columns are the original version (station-corrected data) and corresponding spherical harmonic smoothing of degrees 0-6. The correlation coefficients r between each prediction and the observed, original or smoothed, are also shown at the lower-left corner of each prediction. This event is the same as *Creager and Jordan*'s [1986] Mariana event 2. Our spherical harmonic smoothing is similar to their filtered results. As these authors suggested, the observed residual spheres of this event (top row) exhibit a strong, consistent slablike signature, as expected from its depth. Note, however, that part of the slablike signal is of upper mantle (plus signs away from the slab trend) and deep mantle origin (circles along the trend of the slab; plus signs away from the slab trend). Besides the upper and middle mantle predictions, the deep mantle also exhibits a similar pattern to the observed, i.e., early arrivals along strike and late arrivals in the ESE direction. Slab-like signature in the middle mantle prediction is quite weak (the velocity model has patches of fast heterogeneities around 650 to 800 km). The slow anomalies in the west direction of the upper mantle and the east direction of the deep mantle are largely responsible for the clear slab pattern in the whole mantle prediction

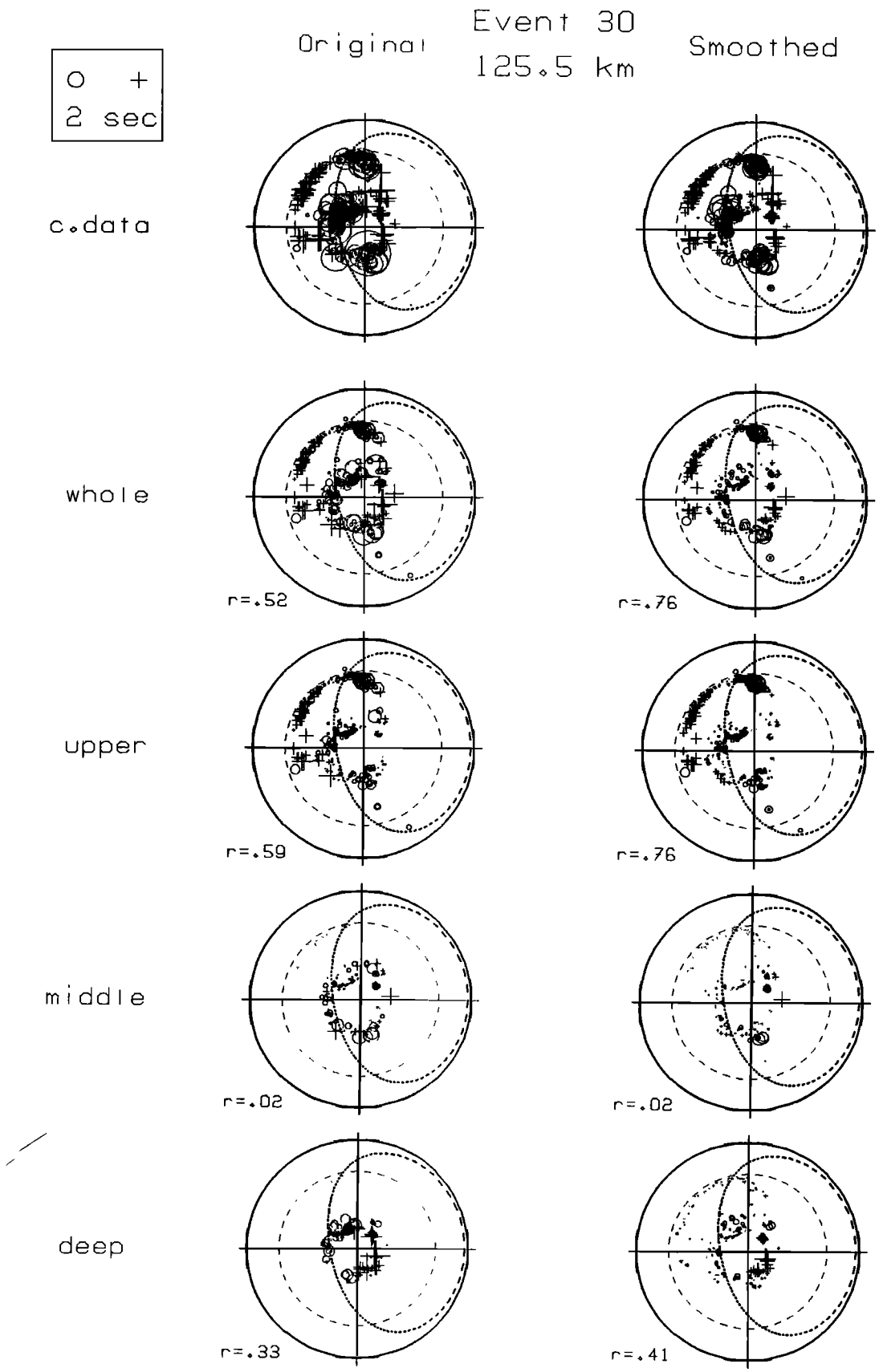

Fig 6. Residual spheres of event 30 Plotting conventions follow that of Figure 5. The event is relatively shallow, and we expect to see the effect of the underlying slab. Indeed, there is a strong slablike signature (fast velocity along the inferred strike direction of the slab) which is mainly caused by the upper mantle. Although an underestimation of magnitude in the velocity models may reduce the contributions from the middle and deep mantle, the middle mantle contributes less than the deep mantle does. The whole mantle model duplicates well the observed pattern and has a correlation coefficient of 0.76 in smoothed versions

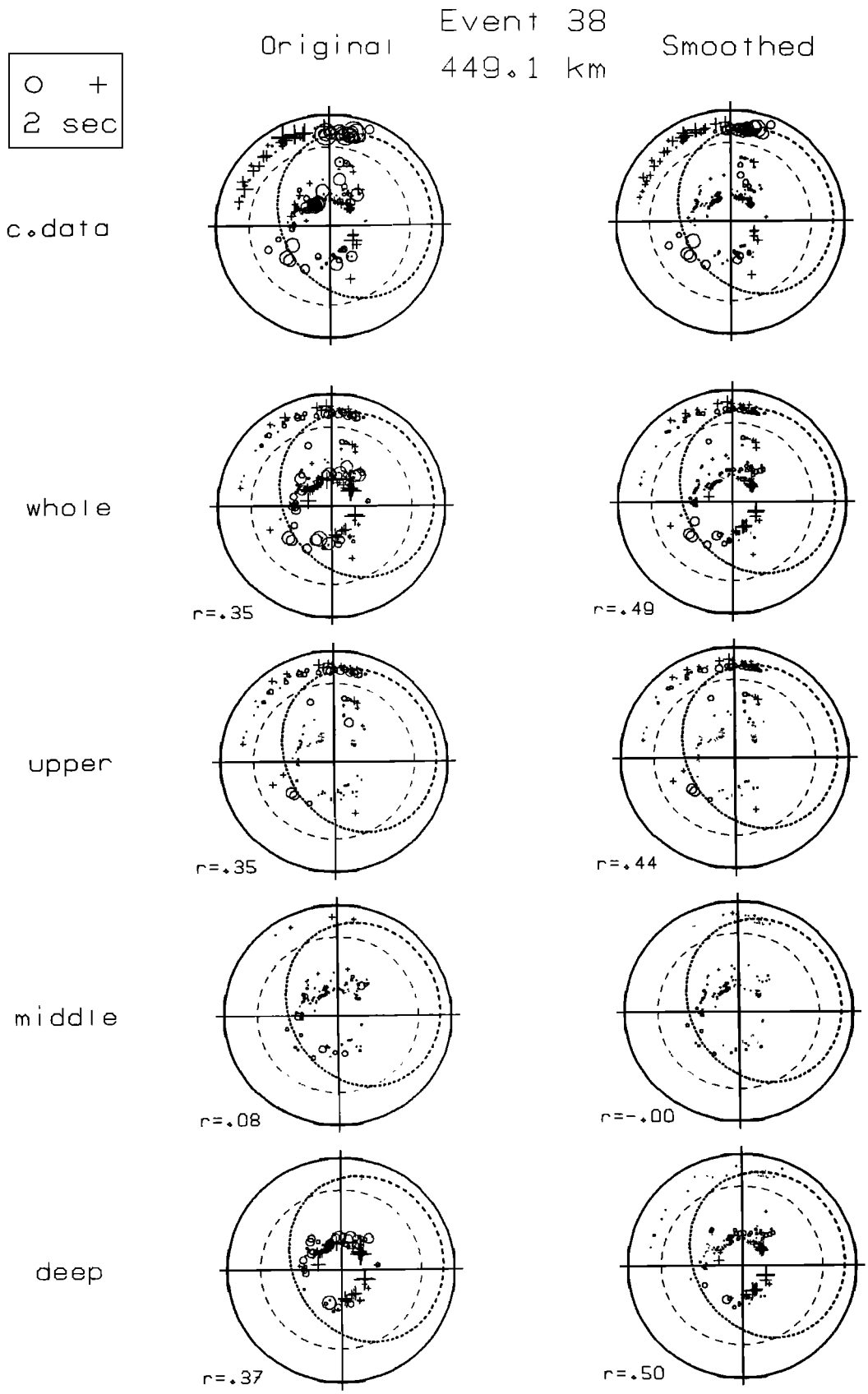

Fig. 7. Residual spheres of event 38. Plotting conventions follow that of Figure 5. This is is an example of a deep focus event that does not exhibit a clear slablike signature. The pattern of arrivals near the center of the residual sphere is controlled by lower mantle effects while the pattern around the edge of the sphere is controlled by the mantle above 650 km. These patterns, however, do not follow slab seismicity trends. Note that the observed lower residual sphere data of this and the next two events actually show a fast residual "ring" in the lower focal spheres, indicating a fast subhorizontal layer lying beneath these earthquakes. This would disappear with the cosine weighting of Creager and Jordan.

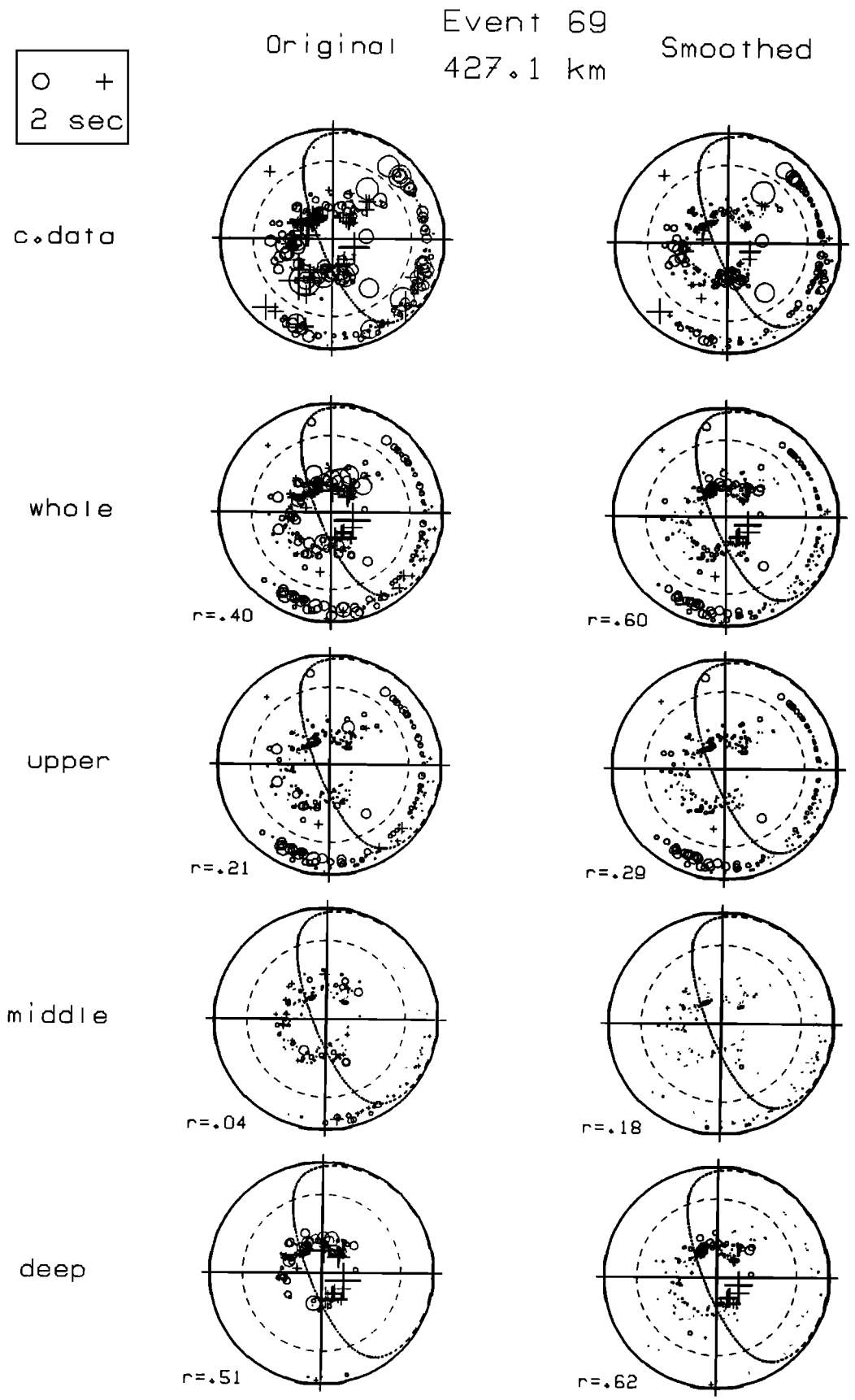

Fig. 8. Residual spheres of event 69. Plotting conventions follow that of Figure 5. Short-wavelength variations appear in data and all predictions. No clear steeply dipping slablike feature is found in either the data or the predictions for this event under central Japan.

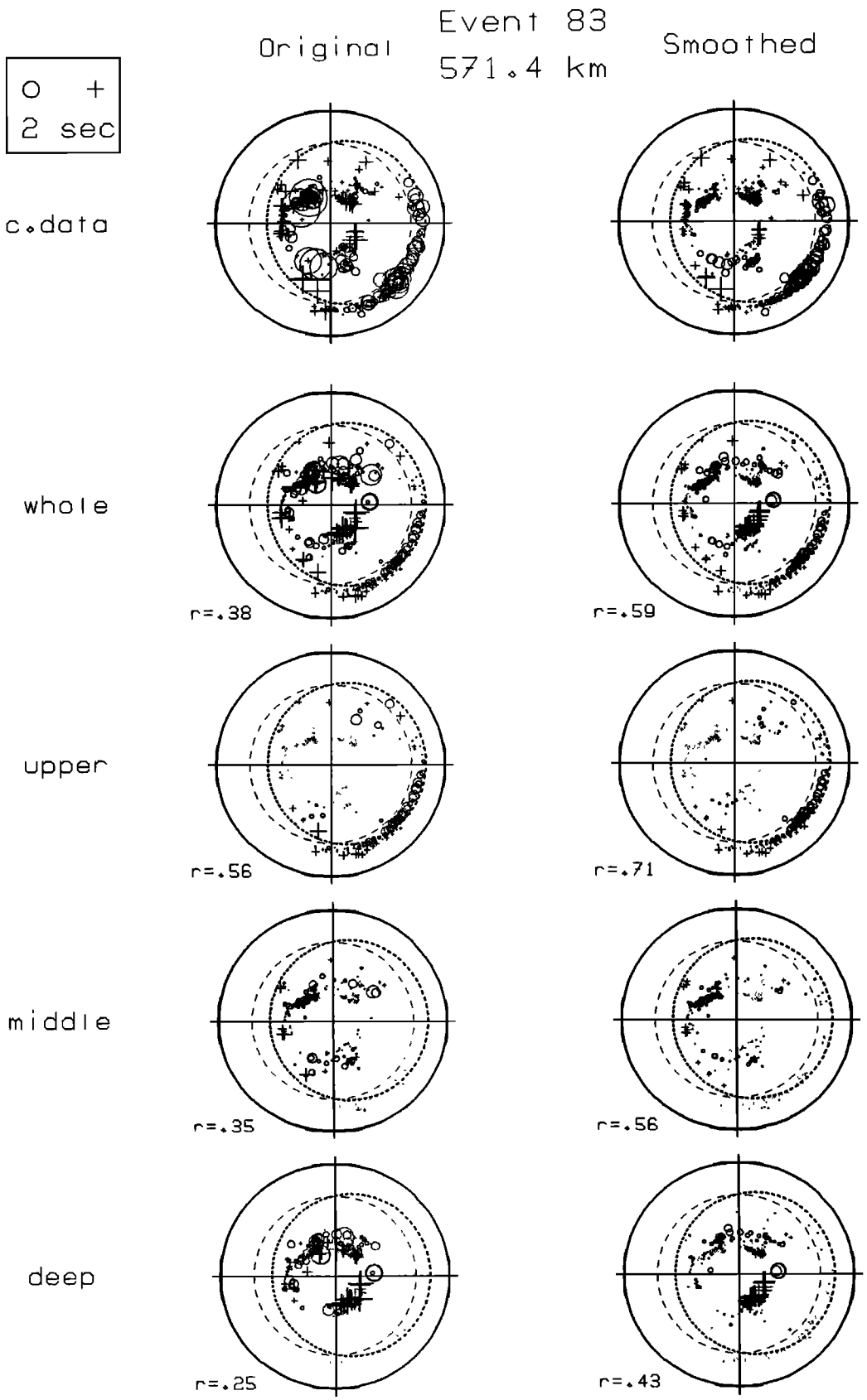

Fig. 9. Residual spheres of event 83. Plotting conventions follow that of Figure 5. This is the same as *Creager and Jordan*'s [1986] event 8. There are fast anomalies of about equal magnitudes in all four quadrants of the middle mantle prediction, reflecting the existence of a subhorizontally lying fast anomaly in the regional model extends to about 800 km depth in this area. The generally fast north and NW quadrants and slow SE quadrant in the deep mantle prediction is more-or-less slablike. On the other hand, the most dominate fast band in the observed residual sphere is subhorizontal. This was overlooked in the Creager and Jordan study because of their restriction to steeply dipping features.

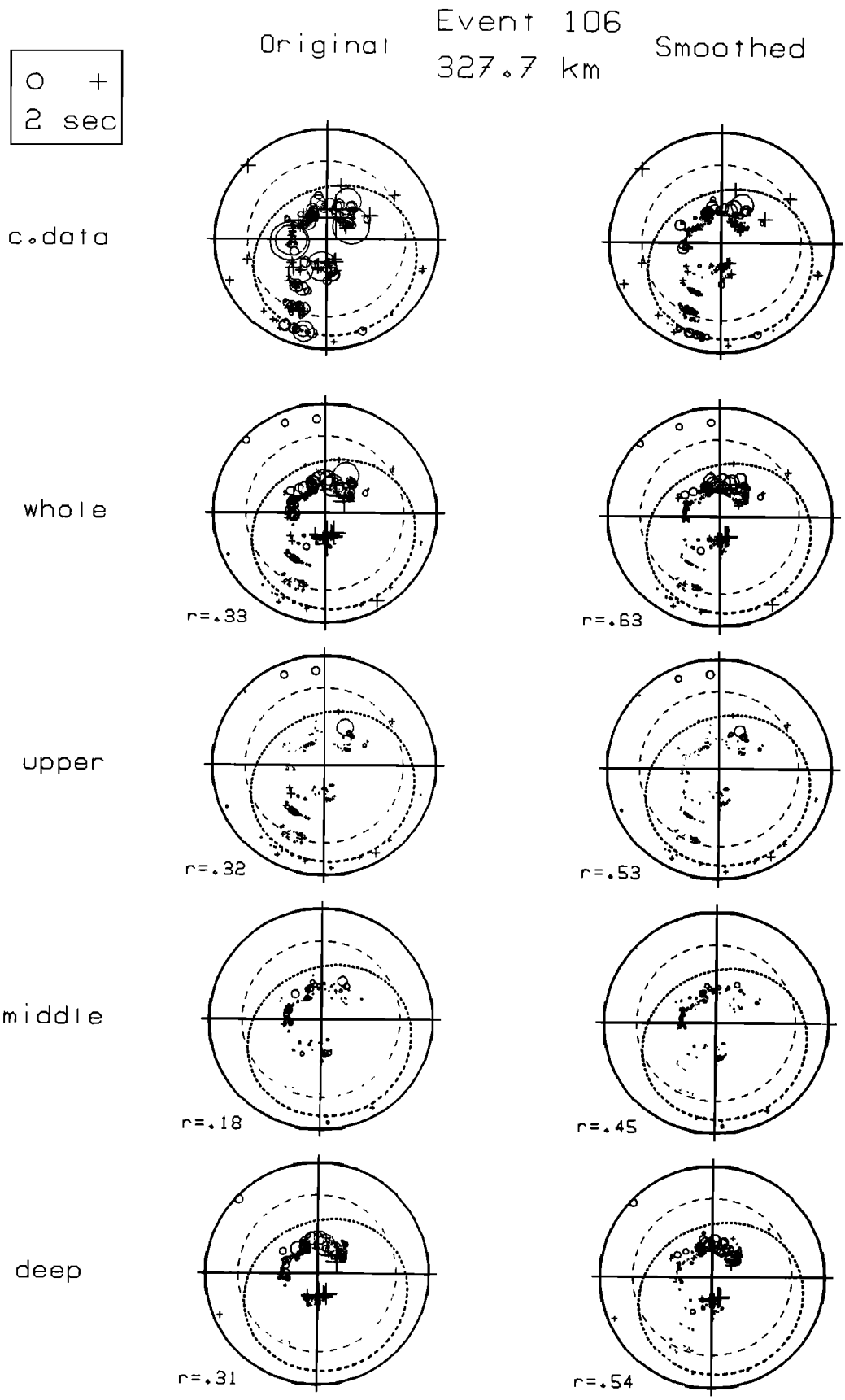

Fig. 10. Residual spheres of event 106. Plotting conventions follow that of Figure 5. The event displays a band of fast residuals which is made up of separate contributions from the deep mantle and the upper mantle. The middle mantle, although slablike, has very minor effect on the whole mantle pattern. The apparent slablike signature in the whole mantle prediction is an artifact of this accidental alignment.

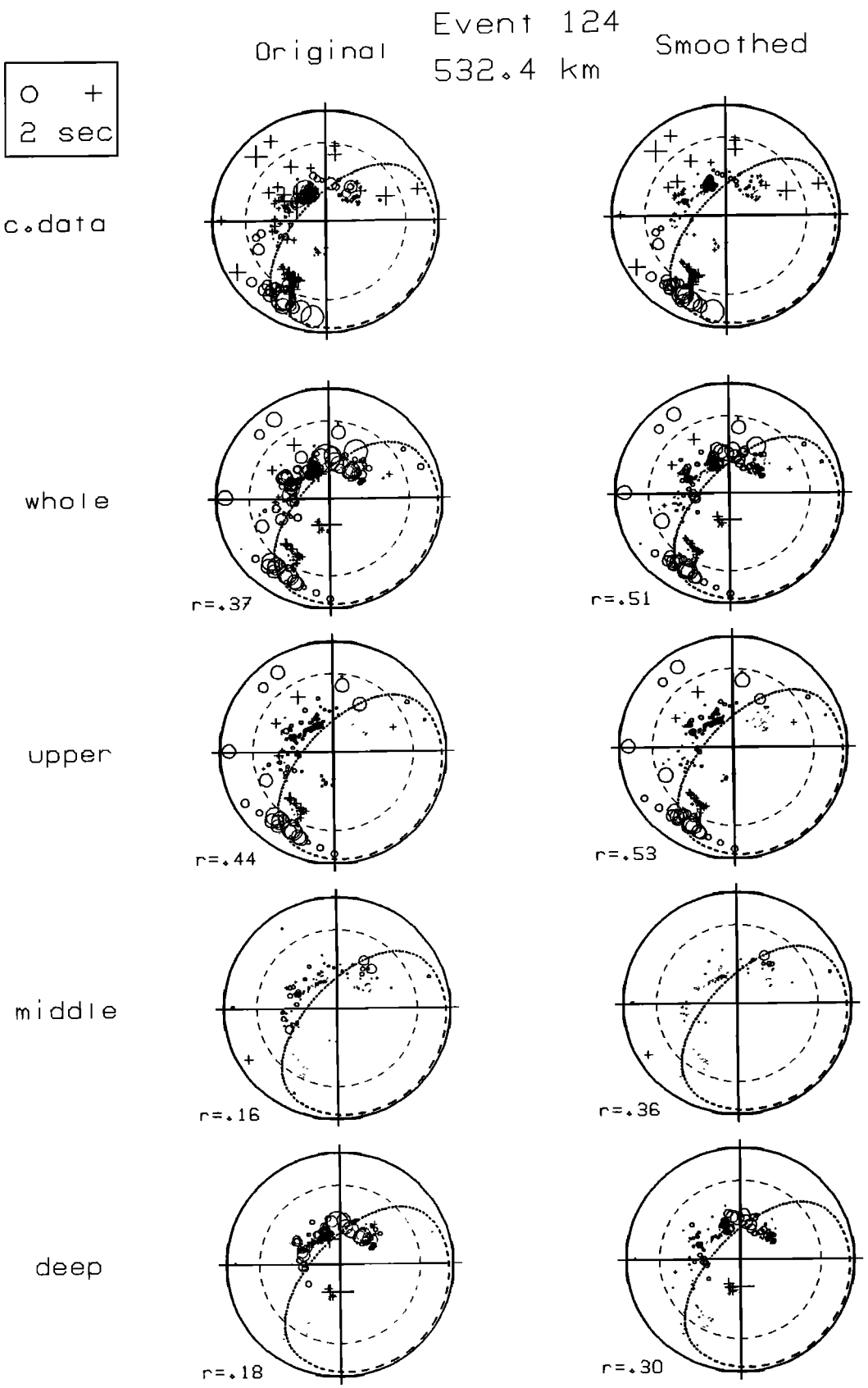

Fig. 11. Residual spheres of event 124. Plotting conventions follow that of Figure 5. The event exhibits a pronounced slablike signature with the expected trend in both data and whole mantle prediction. However, decomposition of the computed residuals into upper, middle, and deep mantles shows that the fast velocities along the trend of the slab in the NE quadrant come from below 1500 km depth, while the fast arrivals in the SSW and ENE directions come from above 650 km. The middle mantle contribution is relatively small.

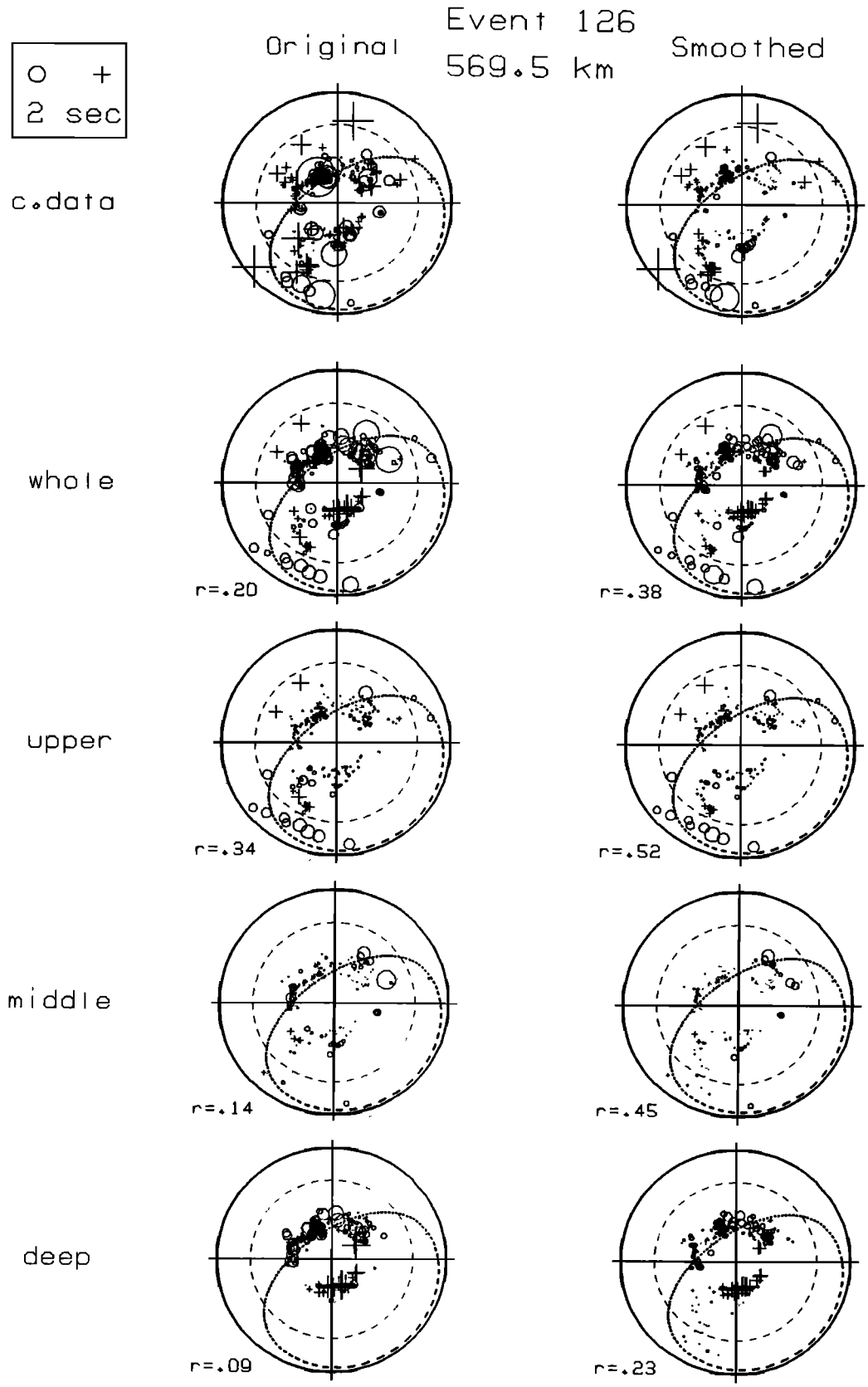

Fig. 12. Residual spheres of event 126. Plotting conventions follow that of Figure 5. There is a strong slablike signature with the appropriate orientation of the deep seismic zone. The integrated effect of the deep mantle accounts for the fast velocities in the northern quadrants and slow in the southern quadrants, while the mantle above 650 km gives slow in the NW quadrant and enhanced the fast slablike trend in the whole mantle prediction. The middle mantle pattern is flat and has a minor role on the whole mantle slablike signature. This is the same as *Creager and Jordan*'s [1984] Sea of Okhotsk event 6, one of the events used to infer slab penetration below 1000 km. Our results show that most of the slablike signal comes from between 1500 km depth and the receivers and where rays have spread out of any source slab.

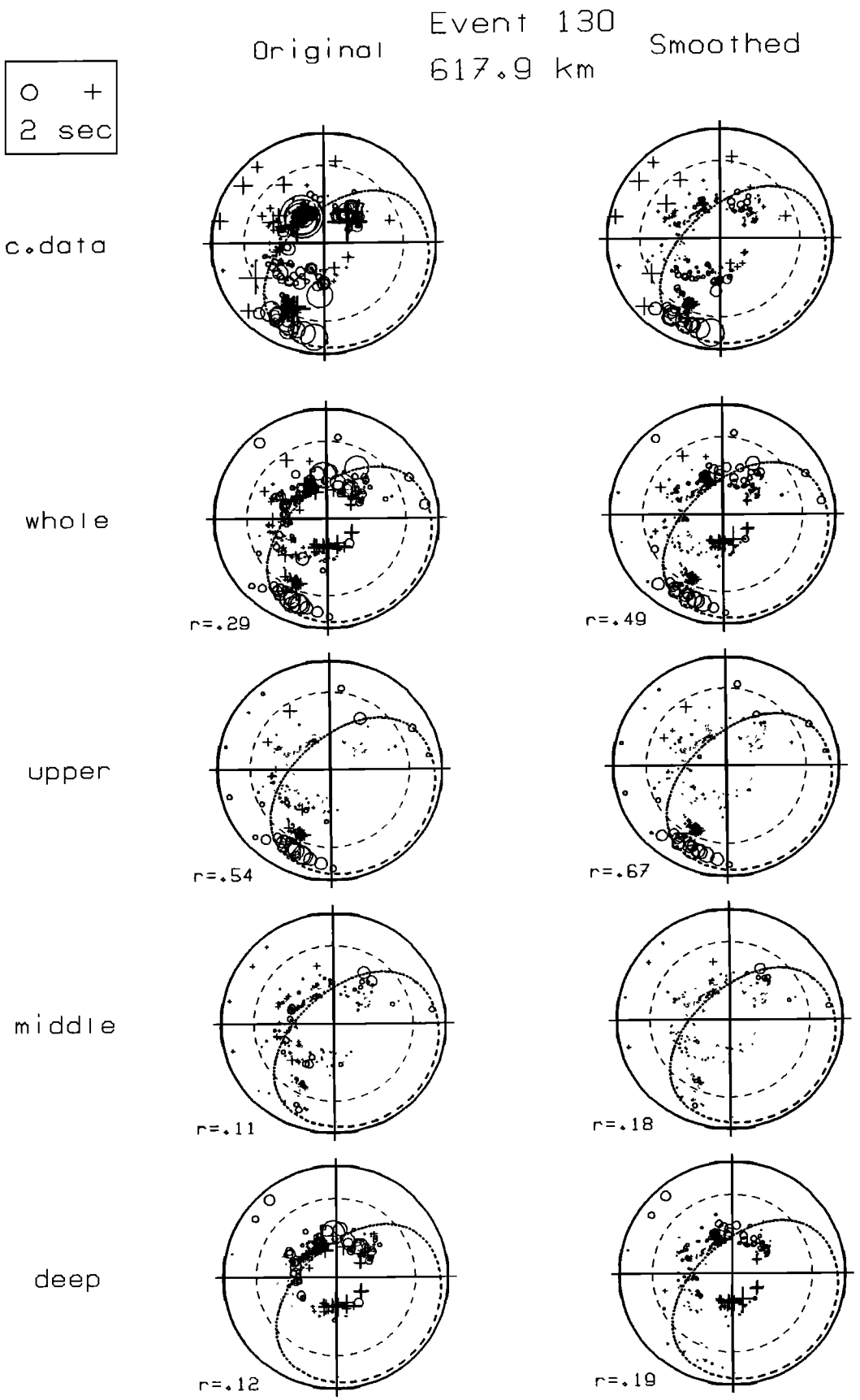

Fig. 13. Residual spheres of event 130. Plotting conventions follow that of Figure 5 This has one of the clearest slablike signature for a deep focus event. The decomposed residual spheres, however, suggest that the deep mantle, which is away from the Kuril subduction zone, plays a major role. The middle mantle residual sphere again has a diffuse look

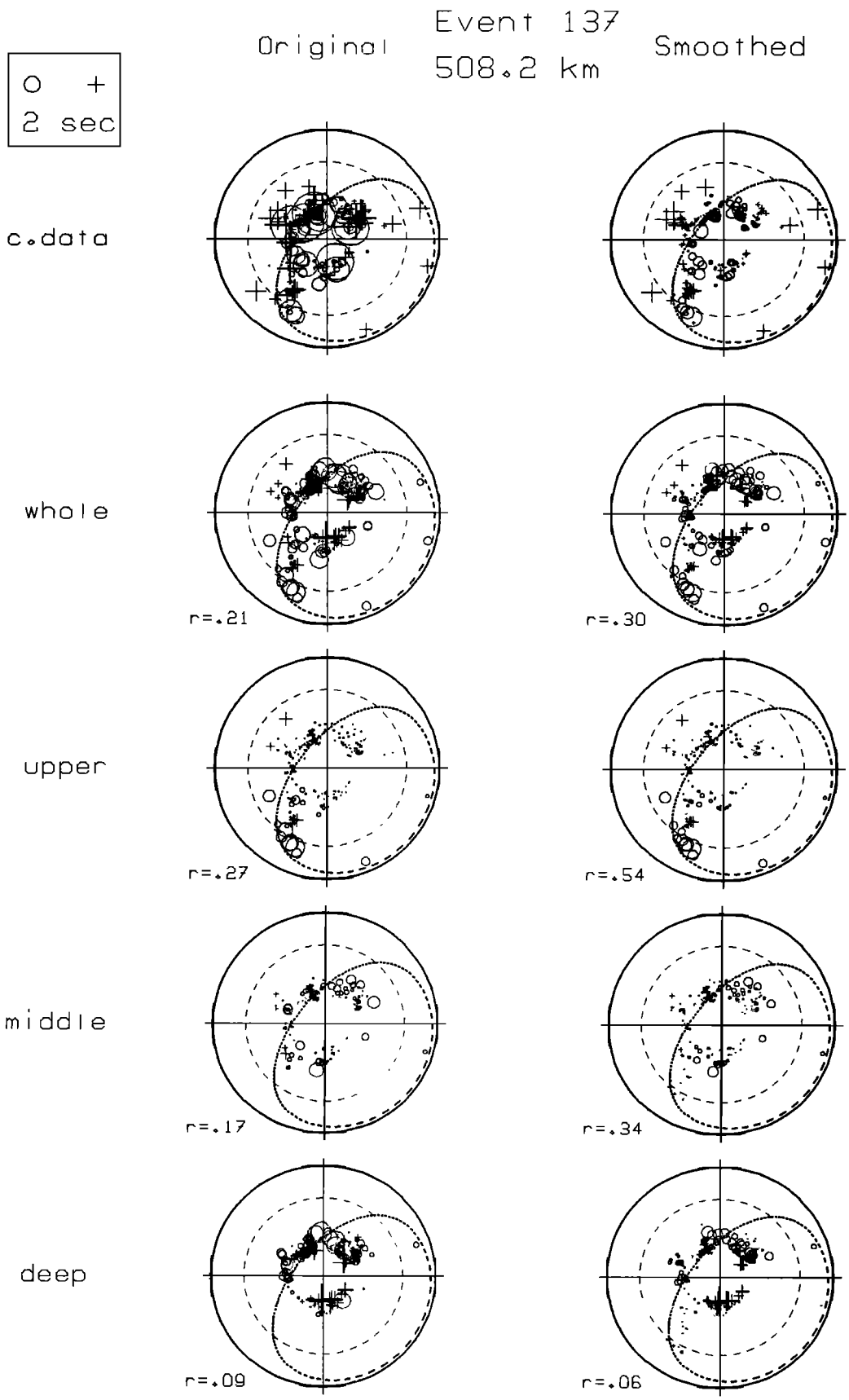

Fig. 14. Residual spheres of event 137. Plotting conventions follow that of Figure 5. This is the same as *Creager and Jordan* [1986] event 6 and the comments made for event 126 (Figure 12) also apply here. The deep mantle plays an important role, as usual, and many residual sphere anomalies are explained by the velocity maps in Figure 3.

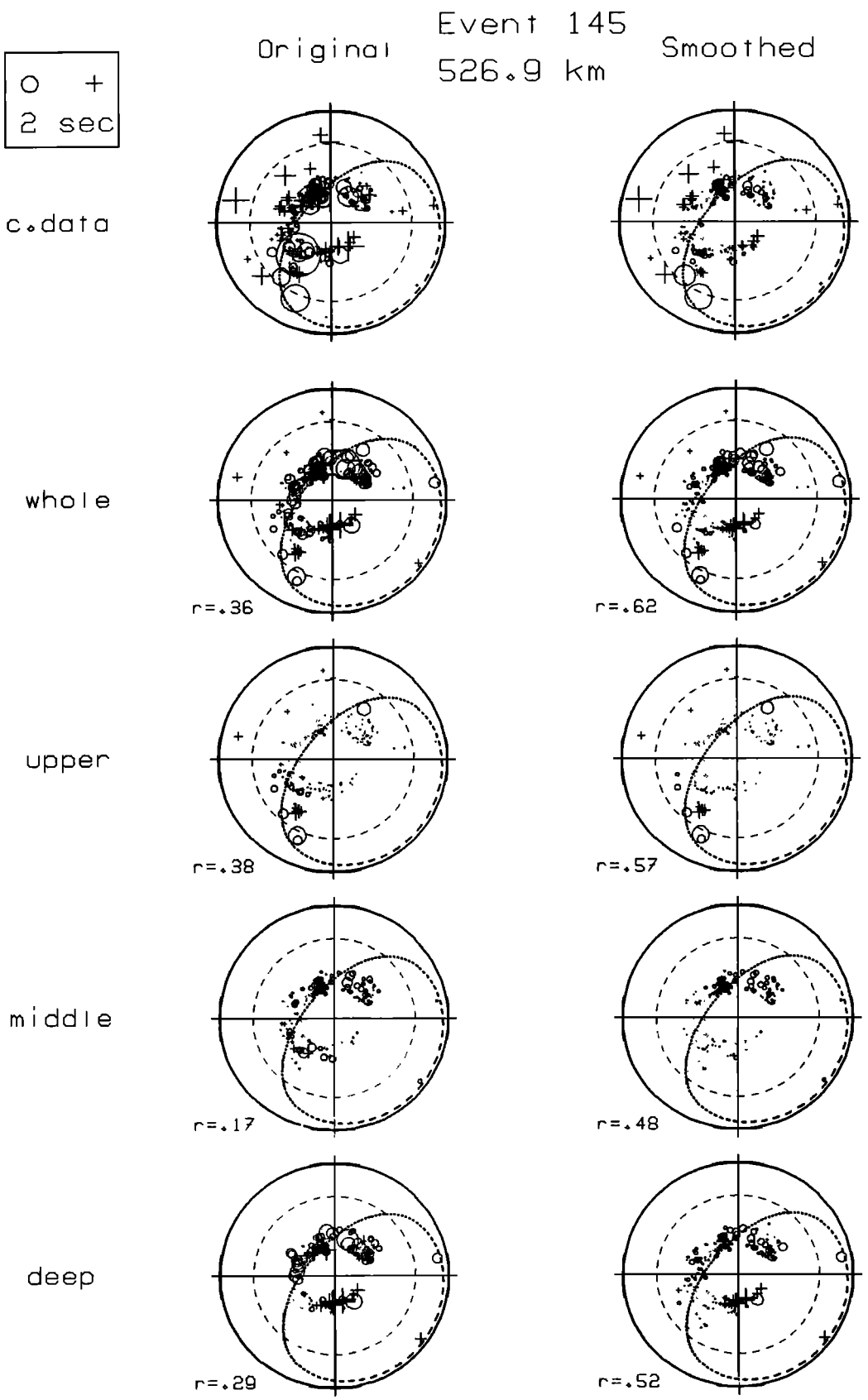

Fig. 15. Residual spheres of event 145. Plotting conventions follow that of Figure 5. This event displays a discontinuous band of fast residuals, a northern clump, and a SW clump. The former is mainly due to deep mantle propagation while the latter is primarily due to the mantle above 650 km. Together they combine with a rather flat middle mantle to give a slablike anomaly. Note the importance of the slow clump in the southern quadrants of the deep mantle, in canceling the fast arrivals in the middle mantle away from the seismicity trend.

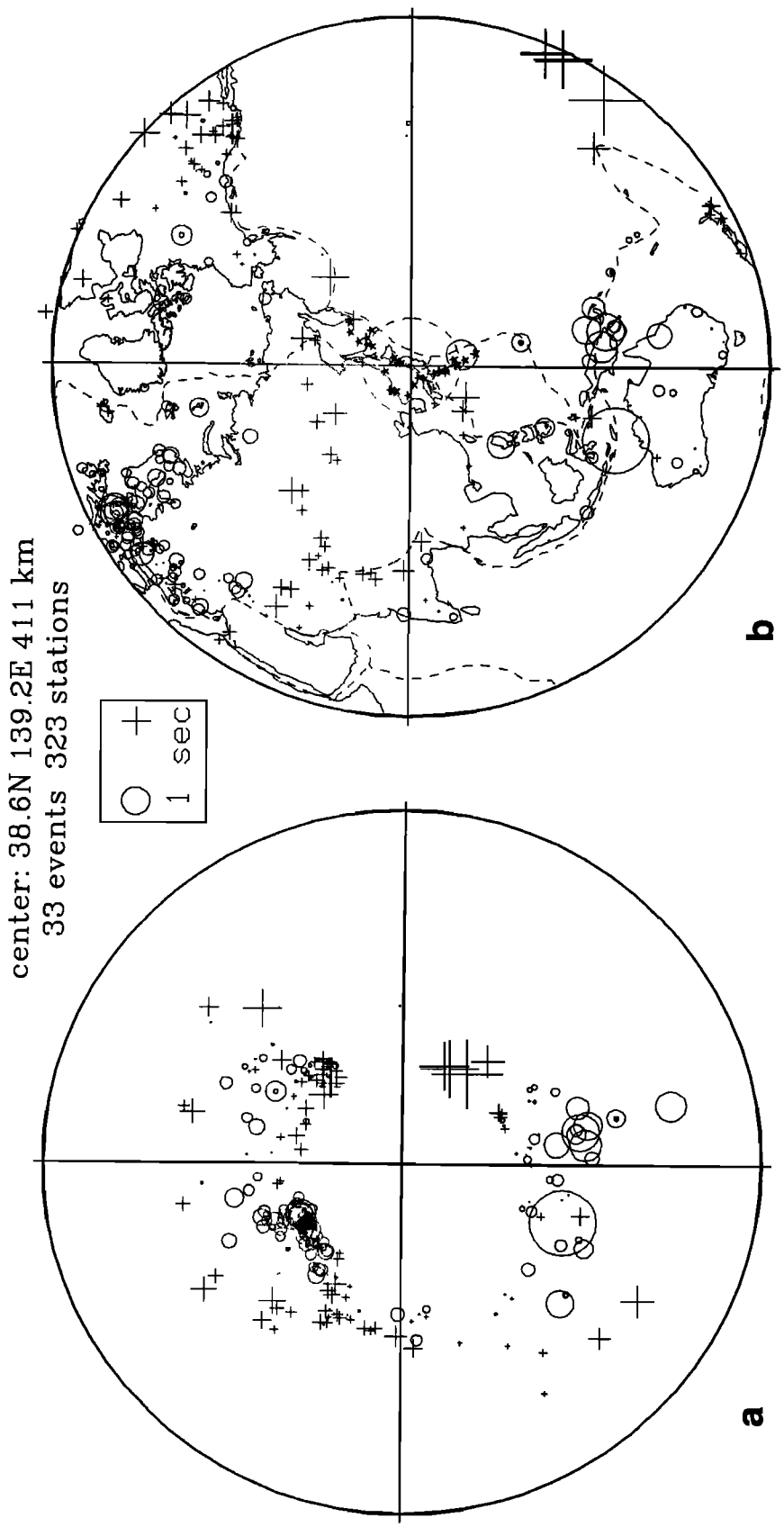

Fig. 16. A test of deep mantle and near-station velocities. Plotting conventions for this Figure is similar to that for the top two small spheres in each panel of Figure 3. The circumference in residual sphere (*a*) corresponds to takeoff angle of 90°, the corresponding epicentral distance in the station location sphere (*b*) is shown by a dashed circle near the center. The small solid stars in Figure 16*b* denote events used in this test, which is discussed in section 4.

residuals at a station includes only the effect of shallow heterogeneities beneath the station.

The test thus confirms the suggestion of a significant effect on the residual spheres by deep diffuse and receiver mantle anomalies. Furthermore, the pattern in Figure 16*a* is more-or-less "slablike" with a north-south trough of fast trend. This pattern is quite similar to the smoothed data by *Creager and Jordan* [1986] for their events 6, 7, and 8, as well as to smoothed data and lower mantle prediction of most events in this paper (see Figures 6-10, 12, 13 and 15). The long-wavelength deep mantle and receiver mantle heterogeneities plus uneven and sparse distribution of seismographic stations make it very difficult to isolate near-source effects by residual sphere techniques.

5 DISCUSSION

Earlier work on the fate of the subducting slab involved the analysis of residual sphere data alone [*Jordan*, 1977; *Creager and Jordan*, 1984, 1986]. Penetration of lithospheric slabs into the lower mantle was proposed. However, raw residual sphere data are extremely noisy, a fact not readily apparent from published data which are heavily smoothed. The interpretation of raw or smoothed residual spheres is not unique since the pattern can be caused by velocity heterogeneities other than subducted slabs. In fact, high-velocity trends on the residual sphere can be due to (1) near-source fast anomalies such as extensions of the slab or, in a layered mantle, thermal coupling between the upper and lower mantles, (2) near-source anisotropy, due to shear induced alignment of anisotropic crystals in the slab or in the mantle surrounding the slab, (3) deformation of interfaces or phase-change boundaries, (4) large-scale coherent structures in the lower mantle which define bands when projected onto the focal sphere, and (5) large-scale structures in the upper mantle beneath the recording stations.

Attempts are made to remove the latter effect (near-station effects) by removing station corrections from the data. However, results in the previous section indicate that a station correction term obtained from a global data base may include only the effect of a shallow region beneath the station. A one-sided upper mantle near-receiver heterogeneity is not removed by standard station corrections.

Travel time residuals integrated through different portions of the mantle model help us to isolate the locations of major velocity heterogeneities causing slablike residual sphere patterns. For the deeper earthquakes we conclude that a substantial contribution to the residual sphere occurs far from the source (deep mantle and receiver mantle). This throws doubt on the interpretation of deep residual sphere anomalies as being almost entirely due to near-source or deep slab effects If the deep mantle and receiver mantle effects can be removed properly, a residual sphere study may give the approximate orientation, but still not the depth extent, of near-source fast velocities. The complexity of the upper mantle in the northwest Pacific region yields complex residual spheres which exhibit rapid and short-wavelength variations that can alias the smoothed results. In a later paper, we show that the smoothed results are sensitive to parameters such as residual cutoff times, apex angle of the cone used to define the residual sphere and method of correcting for receiver and deep mantle structure.

Following are some points we address in more detail.

Inferred contribution from each portion of the mantle. Among the three portions of the whole mantle model (upper, middle, deep), the upper mantle portion, as expected, shows the strongest slab signature. But the upper mantle model alone generally underestimates the variation on the residual spheres, particularly for deep events.

The middle mantle, depths 650 to 1500 km below the earthquakes, is the region important to the deep slab penetration hypothesis. The top portion of the middle mantle also includes part of the region where flattening and fingering of fast slablike anomalies have been suggested [*Zhou and Clayton*, 1987, 1990]. Correlation coefficients between the data and predictions for the middle mantle model are low for most events (Table 1), indicating that the middle mantle has the lowest contribution to the predicted residual sphere patterns in comparison with upper mantle and deep mantle models. The relatively smaller and more homogeneous residual accumulations in the middle mantle model are often overwhelmed by the contributions from other portions of the mantle since they overlay the same area on a residual sphere. In fact, the middle mantle has lower-amplitude anomalies and exhibits less coherency relative to the upper mantle, while the ray paths in the deep mantle are much longer and more widely separated relative to those in the middle mantle. It should be noted that the "650-km" discontinuity, in a chemically layered mantle, may be much deeper under subduction zones, because of the excess mass of the upper mantle.

For most events that we present, downgoing rays from deep events are primarily perturbed from their normal travel times by the deep mantle (between a depth of 1500 km and the receivers) and are only secondarily affected by middle mantle heterogeneities. The deep mantle predictions of travel time anomalies are often similar to the patterns which would be caused by near-source fast slablike anomalies. This is due to the fact that the long-wavelength heterogeneity of the deep mantle sometimes mimics a long slab when projected onto the residual sphere. The deep mantle model is characterized by low-amplitude but long-wavelength seismic velocity anomalies. For example, most of the lower mantle between the northwestern Pacific and North America or Europe is fast, while paths to the Pacific, New Zealand, and central Asia are slow or mixed (Figures 3 and 16). The anomalies are of small amplitude but are spatially consistent over large areas, and therefore the delay time values accumulate to the level observed in residual sphere projections.

It might seem odd that deep mantle predictions for several events appear to have large degree one components. One may wonder if this a source mislocation effect. Should we remove it? The answer goes back to a consideration of the meaning of low-order terms, particularly with regard to smoothing and to source mislocation.

Consider a simplified case. A ray of a path length l passes through both the true and assumed source locations which differ by a length δl. In our computation, the effect of δl on the observed residual is $dt = \delta l * S$, but the effect on model predicted residual is $dr = \delta l * dS$, where S and dS represent

slowness and its perturbation. In this regard, dr, the effect of error in the source location on the model prediction, is not the same as the conventional mislocation term dt. The former is smaller than the latter by a factor of dS/S (usually less than 10% for deep earthquakes). Because dt and dr are different, we cannot compare the amplitude of the observed and predicted residual spheres without removal of the degree zero and one terms. To compare the predicted relative amplitudes among the different fractions of mantle, however, we only have to consider the error contribution $dr = \delta l * dS$. The dr is commonly 1 order of magnitude smaller than the deep mantle prediction whose peak-to-peak value exceeds 2 s ($dr = 0.1$ s if $dl = 10$ km and a 10% perturbation exists on a S of 10 s/km, and each event used has been well recorded and relocated).

Valid residuals, due to real mantle heterogeneity, can be mapped onto a residual sphere as a degree one term. Only a fraction of the whole mantle is considered here, and degree one contributions from different fraction can be integrated to form higher-degree anomalies. In addition, most of the effect of δl is on the prediction of the near-source upper mantle or middle mantle but not on that of the teleseismic deep mantle. Based on these considerations, we can compare amplitude contributions predicted from different portions of the mantle without worrying about contamination from source mislocation of the given events.

For deep mantle propagation from the Mariana source region (e.g., Figure 5), about 1-s negative (fast) residuals accumulate in the NW (European) and SE (New Zealand, eastern Australia) quadrants, while most easterly and ESE directions (central Pacific) are slow. These anomalies combine to give a trend, as mapped on the focal sphere, approximately the same as the trend of the northern part of the Mariana arc. They are, however, unrelated to present subduction under the Mariana trench Even though we know that there are some fast heterogeneities in the top portion of the middle mantle in this area, the fast band in the residual sphere is contaminated by the deep mantle contribution. In northern Japan the data exhibit a continuous band of fast arrivals in the northern quadrants (northern Europe, Canada) extending from West to NE. This is due to the fast deep lower mantle encountered by rays going to these locations. For events in the Kuril-Kamchatka area the deep mantle contributes mostly fast velocities in the northern quadrants and slow velocities to the south and southeast (New Zealand to the central Pacific), which is also evident in the velocity maps of Figure 3. The upper mantle contributes to the fast arrivals in the SW quadrant (India and southeast Asia), which combine with the deep mantle and, to a lesser extent, the middle mantle anomalies to give the appearance of a continuous fast band having more-or-less the trend of the arc in this region.

Reliability of the mantle P wave models. The major finding in this study is that apparent slablike patterns in residual spheres may be caused by diffuse mantle heterogeneities rather than subducted slabs. The relative influence levels of slabs and other heterogeneities may vary at different locations. Although the above finding has been confirmed in section 4, it also quantitatively depends on the velocity model, particularly the regional model, used. The reliability of the regional mantle model of *Zhou and Clayton* [1990] is discussed at great length in the original paper (also by *Zhou* [1988]). They calculated resolution and did tests on synthetic models and also derived similar P wave and S wave structures. The residual spheres that includes rays of takeoff angle greater than 90° (the upper hemisphere) provide additional confirmation of this model.

In most mantle velocity tomographic inversions, the amplitude of heterogeneities at depth is probably underestimated. For our modeling, the underestimation will primarily effect predictions from middle mantle and deep mantle models. In this sense, the ratio between residual sphere predictions from the middle mantle and deep mantle models may be less affected. In addition, the magnitude of the predicted residual spheres for most events in this study are comparable to that of the observed, indicating that the magnitude underestimation for the current study is perhaps not too serious.

The large fast heterogeneity pattern in our deep mantle model, taken from *Clayton and Comer* [1983], is also evident in the studies of *Dziewonski* [1984], *Hager et al.* [1985], and *Dziewonski and Woodhouse* [1987]. The origin of these large heterogeneities is unknown, but we can rule out the possibility that they are totally artifacts from the inversions because (1) similar patterns are not observed in the middle mantle model; (2) crossing rays used in the construction of the deep mantle model are from many more sources and receivers than only those of the northwest Pacific subduction region; and (3) the dominant fast trend in the pattern does not always agree with the strike of the northwest Pacific subduction zone, due to the geometrical variation of the latter. Nevertheless, the pattern usually gives a long-wavelength signature to residual spheres, at least in our present study region, which has about the trend of the northwest Pacific subduction zones. It is not always appropriate, therefore, to attribute the long-wavelength part of the residual sphere to near-source effects. Conventional smoothing of residual sphere data is not adequate to resolve the location of the mantle anomaly.

Items 1 and 2 above make it less likely that upper mantle or near-source anomalies are severely projected into the lower mantle, a real danger if only earthquakes from our study region were used in the lower mantle tomography. Normal residual sphere analyses, in particular, have this defect, having no crossing rays to cancel out projected near-source artifacts.

About shear waves. Tanimoto [1989] has recently derived an S wave structure for the whole mantle using SH body waves and long-period Love waves. From a depth of 1600 km to the core-mantle boundary the lower mantle is fast beneath most of the subduction zones of the western Pacific. Furthermore, great circle paths along strike of the NW Pacific subduction zones travel in faster than average velocity in the lower mantle and emerge through faster than average upper mantle under North America and SE Asia. The lateral variations are of the order of 0.5-1%. A similar pattern is found in the lower mantle shear velocity model displayed by *Dziewonski and Woodhouse* [1987]. For lower mantle shear wave travel times of 500 s this would give anomalies of 2.5-5 s. This is a large fraction of the variation actually observed on an S wave residual sphere [*Jordan*, 1977] and which has been attributed to deep slab penetration.

Most of the power in the long-wavelength variation of the lower mantle is in harmonics of degree 1, 2, and 3 [*Tanimoto*, 1989]. This long-wavelength power maps onto the residual sphere as long-wavelength anomalies. Thus the basic assumption of the deep slab penetration hypothesis, namely, that long-wavelength variations on the residual sphere are due to near-source velocity anomalies, is false. We have already pointed out that near-source structure contains appreciable short-period power.

In the first *S* wave study of residual spheres in the Sea of Okhotsk area, *Jordan* [1977] noted that in the NW and SE quadrants the residuals are generally positive, whereas in the NE and SW quadrants the residuals are generally negative. "The broad spatial coherence of this pattern suggests the existence of velocity heterogeneity in the vicinity of the source." We get exactly the same pattern in this region for the deep mantle model, even though we pick up the integration more than a thousand kilometers below the source. Additional negative residuals are picked up by rays travelling in the upper mantle toward the SW. The combination of the fast patches contributed by the deep mantle and the upper mantle gives the appearance of a single fast band which *Jordan* [1977] interpreted as a slab signature from the middle mantle region.

Previous residual sphere modelings. There have been two previous attempts to compare residual spheres predicted by mantle velocity models with actual residual sphere data [*Dziewonski*, 1984, *Creager and Jordan*, 1986]. It is difficult to judge the reliability of a tomographically obtained velocity model and comparison with residual sphere data is one test of such models. In the above studies the general patterns are similar but the lower mantle model L02.56 (from *Dziewonski* [1984] in each case) predicts residual amplitude much smaller than observed. This is probably due to the damped minimum-norm procedure used to obtain the lower mantle model. This tends to minimize the perturbations. In order to better account for near-receiver upper mantle and to help the reader judge the reliability of the residual sphere predictions we have used a different lower mantle model [*Clayton and Comer*, 1983]. Some details of this model and the procedures used to derive it are from *Hager and Clayton* [1989]. In long-wavelength characteristics it is similar to L02.56 in pattern but different in amplitude [*Hager et al.*, 1985]. Relatively short-wavelength perturbations of the lower mantle, not included in the L02.56 spherical harmonic model (up to degree 6), also contribute to residual sphere anomalies. An anomaly of degree 6 in spherical harmonic expansion has a lateral length of over 50°, certainly not small for residual sphere analysis. The comparison between computed and observed residual spheres for the deeper earthquakes is a direct test of the reliability of the deep mantle model and our results can be compared with similar tests performed in the above mentioned studies

Dziewonski [1984] also showed that the lower mantle was responsible for a large part of the character of the residual sphere. The source region does not generally dominate the large-scale patterns of observed travel time residuals. His lower mantle model, however, underestimates the variation relative to the observations, by about a factor of two. We agree that large-scale structure of the lower mantle is important in the residual sphere at long wavelength. A basic premise of some previous studies is that the long-wavelength pattern is due to near-source structure, in particular, deep slabs. *Creager and Jordan* [1986] explicitly correct for the effects of Dziewonski's lower mantle and conclude that the correction is minor but helps in the variance reduction. In contrast, we conclude that the signature of the lower mantle and near-receiver upper mantle is more likely to be dominant, particularly for the deeper events.

Our computed lower mantle patterns using the Clayton-Comer velocity model have long-wavelength components that are much larger in amplitude than in the Dziewonski model. Dziewonski also points out that his model underestimates the residual sphere variations by about a factor of 2, even in nonslab regions. His method of smoothing and damping is expected to underestimate the total variation, particularly since he uses a minimum-norm inversion algorithm. He also subtracts out the azimuthal parts of the station residuals. These are expected to contain much of the information about lower mantle structure. Thus it is perhaps not surprising that correcting for the Dziewonski lower mantle does not affect Creager and Jordan's conclusion about near-source heterogeneity and deep slab penetration.

Creager and Jordan compare their smoothed residual sphere data with the identically smoothed predictions from a slab model. The parameters of the slab model (dip, length, width, depth of penetration, velocity contrast) are adjustable. In most cases there is a nearly perfect fit between smoothed data and smoothed model. Since the unsmoothed data and unsmoothed model are not compared it is difficult to determine if the near-perfect fit is due to an excellent choice of model or due to the heavy smoothing and fortuitous station distribution. Considering the similarity between their raw data and ours, we conclude that the smoothing plays a key role in their analysis and interpretation. Our different conclusions are drawn from basically the same raw data.

The cosine taper in their smoothing operator is particularly suspect. A taper is ordinarily used as a smoothing truncation applied only to the edge portion of a data set. The cosine taper, however, has been applied to the entire model space and is therefore a weighting function. It systematically suppresses or eliminates higher takeoff angle (i.e., shallow dip) anomalies. Beyond the distance of 60°, the Herrin table used by their study has a higher $dt/d\Delta$ gradient relative to the JB table (see Figure 7 of *Herrin et al.* [1968]). This implies that their work may have higher amplitude negative residuals relative to JB times at smaller takeoff angles. The cosine weighting and the exclusion of rays of greater than takeoff angle of 60° tends to produce a higher-amplitude anomaly at a steeper dip, with an orientation dependent on the station distribution. It also eliminate the possibility of finding shallower dipping structures, such as slabs which are confined to the upper mantle or slabs which are deflected to shallow dip by the 650-km discontinuity.

Further comments. There are other limitations to the residual sphere method for detecting the depth extent of slabs. For example, converting a residual sphere anomaly into a statement about penetration depth of the slab requires an assumption about the slab velocity contrast. In

addition, a residual sphere excluding core phases cannot probe narrow regions which are greater than several hundred kilometers beneath the source, because of spreading and refraction of rays and the low density of seismic observations. Therefore, when the subducting slab is not very straight along strike, such as under the Mariana region, or when the dip of the slab is varying or shallow, such as under the Japan Sea, the chance of seeing a clear deep slab signature on the residual sphere is slim. Fast regions of the mantle are antiwaveguides in the sense that rays are refracted out of such regions. A single ray cannot therefore travel very far along a high-velocity slab and a narrow bundle of rays near the source is spread over a large area of the Earth's surface.

The subducting lithospheric slab in the northwest Pacific, as indicated by residual sphere data in this study, may extend below the deepest earthquakes (e.g., under the central Mariana trench). For most deep earthquakes under Japan the predominant fast band is subhorizontal rather than near vertical. Unfortunately, as we have discussed, the depth extent cannot be uniquely determined by the residual sphere method. However, since the mantle velocity models predict the residual sphere data quite well, conclusions regarding the morphology of the deep slab by *Zhou and Clayton* [1987, 1990], particularly the possibility of slab flattening, and either broadening and/or fingering in the transition zone, are strengthened. That is to say, the teleseismic data projected on the residual spheres generally agree with the model predictions which, for the upper and middle mantles, are based on regional data. On the other hand, other pieces of information, such as the decreasing amplitude of the slablike signature with depth in the Mariana residual sphere data which extrapolates to a depth of around 850 km for a fast anomaly, are in agreement with the regional velocity model. The fast heterogeneities in the deeper lower mantle, although having no direct connection with modern subduction zones, may be the remains of ancient subducting slabs, detached cold boundary layers from the top of the lower mantle, or simply downwellings in a convecting mantle. Their scale length is much greater than slabs. It may be that downwellings in the upper mantle only occur over broad downwellings in the lower mantle or that descending slabs trigger lower mantle downwellings. Thus, even if fast velocities at the top of the mantle correlate with the locations of subduction zones, there are explanations other than deep slab penetration.

6. CONCLUSIONS

We have analyzed P wave travel time residual spheres of the 145 best observed subduction zone earthquakes along the northwest edge of the Pacific. The observed residual spheres are compared to predictions of a composite upper mantle-lower mantle velocity model, constructed by embedding a regional model into a global mantle model, both from previous travel time inversions. The composite model explains much of the residual sphere data in pattern, including some short-wavelength features, and in amplitude. This modeling approach is suggestive as to the locations of the mantle heterogeneities that cause the residual sphere anomalies. The predicted residual spheres for the upper mantle model alone do not, in general, explain the pattern or amplitude of the observed residual spheres, particularly for the deeper events. The region immediately below the deepest earthquakes, depths from 650 to 1500 km, usually does not control the residual sphere pattern, having an effect comparable to or smaller than the effect of the remaining mantle regions. It is shown that many residual sphere anomalies, similar to the expected signature of a fast subducting slab, are actually caused by diffuse deep mantle and near receiver heterogeneities that have no clear connection with a deep slab near the source. Without correcting for these teleseismic effects, it is impossible to determine even the orientation, much less the depth extent, of the subducting slab based on travel time residual spheres alone. In a separate study [*Zhou and Anderson*, 1989] we show that the magnitude and orientation of the best fitting slablike band of fast residuals depends on such arbitrary parameters as cutoff ranges for residual magnitude and takeoff angle and on details of the deep mantle and receiver mantle corrections. In general, the magnitude of the steep slablike signal is considerably decreased by non-near-source corrections, and it is generally within the noise level for deeper earthquakes.

Acknowledgments. This research was supported by National Science Foundation grants EAR 83-17623 and EAR 85-09350. Contribution No. 4585, Division of Geological and Planetary Sciences, California Institute of Technology.

REFERENCES

Clayton, R.W., and R.P. Comer, A tomographic analysis of mantle heterogeneities from body wave travel times, *Eos Trans. AGU, 64*, 776, 1983.

Creager, K. C., and T. H. Jordan, Slab penetration into the lower mantle, *J. Geophys. Res., 89*, 3031-3049, 1984.

Creager, K. C., and T. H. Jordan, Slab penetration into the lower mantle beneath the Mariana and other island arcs of the northwest Pacific, *J. Geophys. Res., 91*, 3573-3580, 1986.

Davies, D., and D. P. McKenzie, Seismic travel-time residuals and plates, *Geophys. J. R. Astron. Soc., 18*, 51-63, 1969.

Dziewonski, A. M., Mapping the lower mantle: determination of lateral heterogeneity in P velocity up to degree and order 6, *J. Geophys. Res., 89*, 5929-5952, 1984.

Dziewonski, A. M., and Don L. Anderson, Travel times and station corrections for P waves at teleseismic distances, *J. Geophys. Res., 88*, 3295-3314, 1983

Dziewonski, A. M., and F. Gilbert, The effects of small, aspherical perturbations on travel times and a re-examination of the corrections for ellipticity, *Geophys. J. R. Astron. Soc., 44*, 7-17, 1976.

Dziewonski, A. M., and J. H. Woodhouse, Global images of the Earth's interior, *Science, 236*, 37-48, 1987.

Hager, B. H., and R. W. Clayton, Constraints on the structure of mantle convection using seismic observations, flow models, and the geoid, in *Mantle Convection*, edited by W. R. Peltier, pp. 657-763, Gordon and Breach, New York, 1989.

Hager, B. H., R. W. Clayton, M. A. Richards, R. P. Comer, and A. M. Dziewonski, Lower mantle heterogeneity, dynamic topography and the geoid, *Nature, 313*, 541-545, 1985.

Herrin, E., W. Tucker, J. Taggart, D. W. Gordon, and J. L. Lobdell, Estimation of surface focus *P* travel times, *Bull. Seismol. Soc. Am., 58,* 1273-1291, 1968.

Jordan, T. H., Lithospheric slab penetration into the lower mantle beneath the Sea of Okhotsk, *J. Geophys., 43,* 473-496, 1977.

O'Connell, R. J., Pleistocene glaciation and the viscosity of the lower mantle, *Geophys. J. R. Astron. Soc., 23,* 299-327, 1971.

Tanimoto, T., Long wavelength S-wave velocity structure throughout the mantle, *Geophys. J. R. Astron. Soc.,* in press, 1989.

Zhou, H., How well can we resolve the deep seismic slab with seismic tomography? *Geophys. Res. Lett., 15,* 1425-1428, 1988.

Zhou, H. W., and Don L. Anderson, Search for deep slabs in the Northwest Pacific mantle, *Proc. Natl. Acad. Sci. USA, 86,* 8602-8606, 1989.

Zhou, H. W., and R. W. Clayton, Travel-time inversion for P and S velocities beneath the northwest edge of the Pacific: slab fingering? *Eos Trans. AGU, 68,* 1379, 1987.

Zhou, H. W. and R. W Clayton, P and S wave travel time inversions for subducting slab under the island arcs of the Northwest Pacific, *J. Geophys. Res.,* in press, 1990

Don L. Anderson and R. W. Clayton, Seismological Laboratory 252-21, California Institute of Technology, Pasadena, CA 91125.

H. Zhou, Department of Geosciences, University of Houston, Houston, TX 77204.

(Received February 10, 1988;
revised October 9, 1989;
accepted September 21, 1989.)